

Reviewed Preprint
v1 • March 20, 2026
Not revised

✉ For correspondence:

yzhuang@simm.ac.cn

Competing interests: No competing interests declared

Funding: See page 31

Reviewing editor: Neeha Zaidi, Johns Hopkins University, United States

© 2026, Wang et al. This article is distributed under the terms of the [Creative Commons Attribution License](#), which permits unrestricted use and redistribution provided that the original author and source are credited.

Turning aging cells into a live vaccine: engineered senescent cancer cells with adjuvant celecoxib for immunotherapy

Yuewei Wang^{1,2}, Ante Ou^{1,2}, Yanli Luo^{1,2}, Yanrong Gao^{1,2}, Yi Zhang^{1,3}, Linxi Qin^{1,4}, Yongzhuo Huang^{1,2,5} ✉

¹State Key Laboratory of Drug Research, Shanghai Institute of Materia Medica, Chinese Academy of Sciences, Shanghai, China • ²University of Chinese Academy of Sciences, Beijing, China • ³Department of Implant Dentistry, Shanghai Ninth People's Hospital, Shanghai Jiao Tong University School of Medicine College of Stomatology; National Center for Stomatology, National Clinical Research Center for Oral Diseases; Shanghai Key Laboratory of Stomatology, Shanghai, China • ⁴School of Chinese Materia Medica, Nanjing University of Chinese Medicine, Nanjing, China • ⁵Zhongshan Institute for Drug Discovery, SIMM, CAS, Zhongshan, China

eLife Assessment

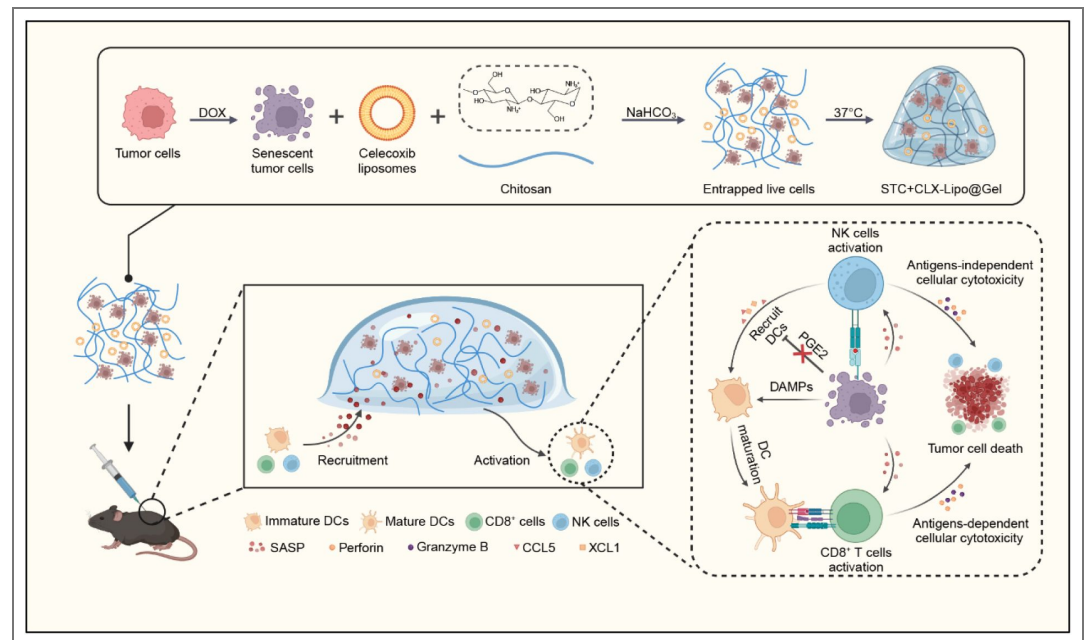
This **important** study presents a novel immunotherapy strategy for cancer. The authors develop a whole-tumor cell vaccine comprised of senescent tumor cells and a COX2 inhibitor in a hydrogel matrix. They present **convincing** evidence of the efficacy of this approach in preclinical models, demonstrating that prostaglandin E2 (PGE2) modulates the senescence-associated secretory phenotype (SASP) toward an immunostimulatory state, although more mechanistic/functional work would strengthen their conclusions. This work is timely and will be of interest to immunologists and others interested in the development of novel cancer therapies.

<https://doi.org/10.7554/eLife.110069.1.sa2>

Abstract

The immunoactivation effects of senescent tumor cells are a potential avenue for cancer therapy. They can act as antigen reservoirs for cancer vaccination, but how to maintain strong immunogenicity to induce a robust immunity is underexplored. In this study, we developed an engineered live vaccine composed of hydrogel-encapsulated senescent tumor cells and liposomal celecoxib (STCs+CLX-Lipo@Gel). This vaccine prolongs the in vivo persistence of senescent tumor cells and utilizes liposomal celecoxib (COX2 inhibitor) to promote the recruitment and maturation of dendritic cells (DC). Notably, a single dose can significantly delay melanoma growth by eliciting robust immunity. The vaccine extended the survival of mice with melanoma brain metastases. Moreover, this strategy also demonstrated high efficacy against orthotopic pancreatic tumors. This study presents a comprehensive strategy to boost the immunogenicity of whole-tumor-cell vaccines by leveraging senescent tumor cells and COX2 inhibition, with treatment efficacy in various tumor models.

Graphic abstract



Graphic summary. Schematic illustration of the preparation of live-cell vaccines and the tumor-specific immune responses elicited by the vaccine. Created with *BioRender.com* [↗](#).

1 Introduction

Whole tumor cell (WTC) vaccines, characterized by their comprehensive antigenic profile, have the potential to minimize tumor immune evasion, but the limited immunogenicity and a rapid clearance of WTC vaccines often results in suboptimal therapeutic responses (Pérez-Baños et al., 2023 [↗](#); Qin et al., 2023 [↗](#); Zhang et al., 2023 [↗](#)). It highlights the need for innovative approaches to enhance their efficacy

Cellular senescence, marked by irreversible cell cycle arrest and a distinctive secretory phenotype, plays a pivotal role in various biological processes, including cancer (Gorgoulis et al., 2019 [↗](#); Marin et al., 2023a [↗](#)). Common anti-cancer therapies—such as radiotherapy, chemotherapy, and immunotherapy—often induce senescence in tumor cells (Gorgoulis et al., 2019 [↗](#); Marin et al., 2023a [↗](#)). While senescent tumor cells (STCs) lose their ability to proliferate, they retain viable state and undergo significant alterations in their surface proteome (Prieto et al., 2023 [↗](#)). Importantly, senescent tumor cells persist and continuously produce antigens over time. Besides, STCs exhibit an altered secretome, termed the senescence-associated secretory phenotype (SASP), which includes pro-inflammatory cytokines and chemokines, enabling the recruitment of various immune cells and initiation of multiple immune responses (Lee and Schmitt, 2019 [↗](#); Park et al., 2021 [↗](#)). It has been demonstrated that the SASP of senescent tumor cells can recruit and activate $CD4^+$ and $CD8^+$ T cells, thereby triggering anti-tumor immunity (Iannello et al., 2013 [↗](#); Marin et al., 2023b [↗](#); Meng et al., 2012 [↗](#); Ruscetti et al., 2020 [↗](#); van Tuyn et al., 2017 [↗](#)). Furthermore, senescent tumor cells release damage-associated molecular patterns (DAMPs), which can effectively recruit dendritic cells (DCs) and promote their maturation, acting as immunoadjuvants (Marin et al., 2023a [↗](#)). The multifaceted role of STCs in modulating the immune response highlights their potential as therapeutic targets and as components of immunotherapeutic strategies.

The alterations of proteome and secretome endow STCs with unique properties that can activate both innate and adaptive immune responses, thus being a “rebel force” against tumor growth (Antonangeli et al., 2016 [↗](#); Antonangeli et al., 2019 [↗](#); Chen et al., 2023 [↗](#); Marin et al., 2023a [↗](#)). For example, drug-induced STCs can upregulate ligands for activating receptors on natural killer

(NK) cells, such as NKG2D and DNAM-1, thus increasing their susceptibility to recognition and elimination by NK cells (Antonangeli et al., 2016 [↗](#); Antonangeli et al., 2019 [↗](#)). Additionally, STCs upregulate MHC1 molecules, enhancing cytotoxic T lymphocyte (CD8⁺ T cell) activity (Chen et al., 2023 [↗](#); Marin et al., 2023a [↗](#)). Moreover, the upregulation of IFN- γ receptor IFNGR1 on STCs makes them highly responsive to IFN- γ and type I IFN signaling, and thus STCs typically enhance MHC1 antigen processing and presentation, further activating CD8⁺ T cells (Chen et al., 2023 [↗](#); Marin et al., 2023a [↗](#)). Due to their distinctive immunogenic properties and a comprehensive antigen profile, STCs have emerged as promising candidates for live whole tumor cell vaccines (Liu et al., 2023 [↗](#); Marin et al., 2023a [↗](#)).

However, there are a primary challenge to overcome. Prostaglandin E2 (PGE2), an essential immunosuppressor secreted by STCs, is prevalent in tumor microenvironment and hampers effective immunoactivation (Bluth et al., 2009 [↗](#); Böttcher et al., 2018 [↗](#); Von Bergwelt-Baildon et al., 2006 [↗](#)). PGE2 can inhibit chemokine secretion by NK cells, as well as the proliferation and maturation of DCs, thus diminishing the cytotoxic efficacy of antigen-specific CD8⁺ T cells (Böttcher et al., 2018 [↗](#); Böttcher and Sousa, 2018 [↗](#); Kyrysyuk and Wucherpfennig, 2023 [↗](#); Wculek et al., 2020 [↗](#)). To address this issue, we proposed a novel vaccination strategy of utilizing STCs as vaccines and meanwhile suppressing PGE2 production for augmenting anti-tumor immune responses.

In this work, we developed a live cell vaccine of STCs and designed a formulation (designated STCs+CLX-Lipo@Gel), in which STCs and liposomal celecoxib were encapsulated into chitosan hydrogel. This design created a niche to prevent STC clearance and extend action duration. Notably, celecoxib is an FDA-approved inhibitor of cyclooxygenase 2 (COX2), and liposomal celecoxib can block COX2/PGE2 pathway to augment the vaccination efficacy. COX2 is a key enzyme controlling PGE2 synthesis, thus serving as a therapeutic target for inhibiting PGE2 production and enhancing immune cell functions (Deng et al., 2022 [↗](#); Jahani et al., 2023 [↗](#)). STCs+CLX-Lipo@Gel was expected to harness the antigenicity and adjuvanticity of STCs to stimulate both innate and adaptive immune responses.

2 Results and discussion

2.1 Activation of anti-tumor immunity by senescent tumor cells

Utilizing doxorubicin as a senescence-inducing agent (Marin et al., 2023a [↗](#)), we demonstrated the successful induction of senescence, evidenced by the upregulation of senescence-associated β -galactosidase (SA β G) activity (Figure 1A [↗](#)) and senescence-associated gene expression (Figure S1A [↗](#)), and the increased production of SASPs (e.g., IL-6 and CXCL1) (Figure S1B [↗](#)). STCs exhibited elevated secretion of ATP and HMGB1, and canonical DAMPs, and notably promoted the differentiation of CD11c⁺ MHCII⁺ DCs (Figure 1B [↗](#) and C [↗](#)). It is widely recognized that cellular senescence leads to alterations of the surface proteome and the release of a spectrum of chemokines and pro-inflammatory cytokines, thereby making them susceptible to immune surveillance and immune clearance (Gasek et al., 2021 [↗](#); Hasegawa et al., 2023 [↗](#)). Our results revealed a marked upregulated expression of immune cell chemokines (CCL2, CCL5) and antitumor cytokines (IFN- γ , IL-2, IL-12, and IL-15) (Supplementary Figure S2A [↗](#) and C [↗](#)); these chemokines are crucial for the recruitment and activation of CD8⁺ T cells and NK cells (Böttcher et al., 2018 [↗](#); Marin et al., 2023b [↗](#); Takasugi et al., 2023 [↗](#)). Additionally, the NKG2D ligand proteins (ULBP1, RAE-1) and DNAM-1 ligand protein (CD155), which are pivotal for the activation of NK cells upon receptor binding (Antonangeli et al., 2019 [↗](#)), were also significantly elevated (Supplementary Figure S2B [↗](#)). Furthermore, STCs coculturing with splenic lymphocytes led to a high activation rate of CD8⁺ T cells and NK cells (Figure 1D [↗](#) and E [↗](#)). The secretion of cytotoxic perforin and granzyme B by these immune cells was significantly increased in the STCs-coculturing group (Figure 1F [↗](#) and G [↗](#)), further indicating an enhanced capacity to kill tumor cells. Our results were in agreement with previous studies that highlighted the interaction of STCs with immune cells (Antonangeli et al., 2019 [↗](#); Böttcher et al., 2018 [↗](#); Marin et al., 2023b [↗](#); Takasugi et al., 2023 [↗](#)).

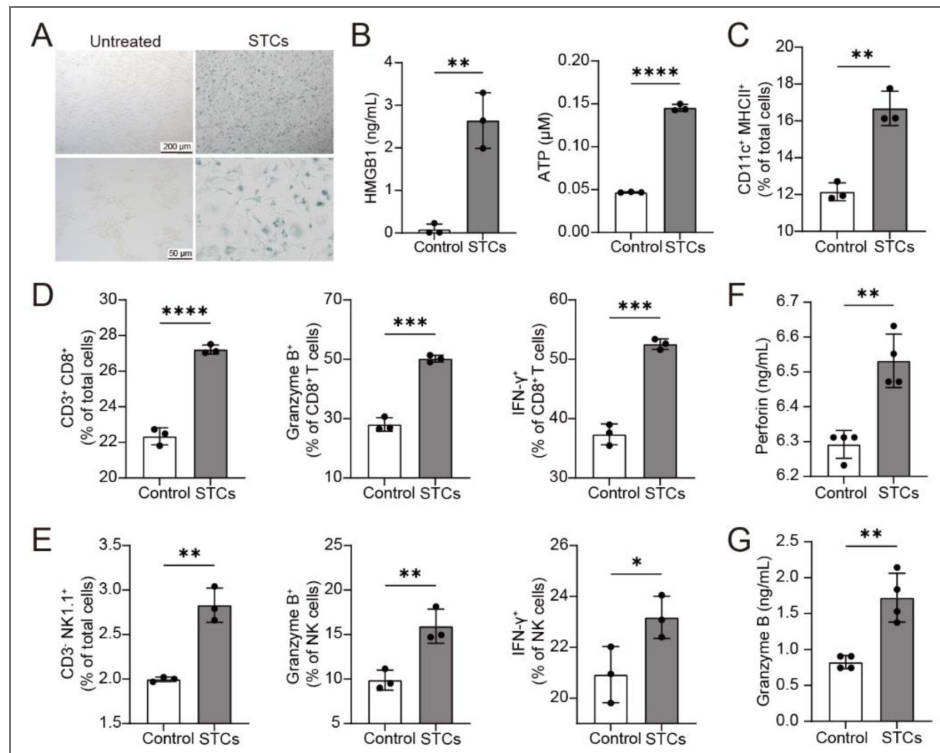


Figure 1. Activated anti-tumor immunity of senescent B16-F10 cells in vitro.

(A) Images of senescence-associated β -galactosidase staining of B16-F10 cells (top panel scale bar: 200 μ m; bottom panel scale bar: 50 μ m). (B) The concentrations of HMGB1 and ATP in the supernatant of untreated cells and STCs. (C) The percentage of CD11c⁺ MHCII⁺ DCs after treatment with untreated cells and STCs. (D) The percentage of CD3⁺ CD8⁺, CD8⁺ Granzyme B⁺ and CD8⁺ IFN- γ ⁺ T cells after treatment with untreated cells and STCs. (E) The percentage of CD3⁺ NK1.1⁺, NK1.1⁺ Granzyme B⁺ and NK1.1⁺ IFN- γ ⁺ cells after treatment with untreated cells and STCs. The concentrations of (F) Perforin and (G) Granzyme B in the supernatant of untreated cells and STCs (n=4). Statistical significance was assessed by unpaired Student's t-test. Data were presented as mean \pm SD. Statistical significance was determined as *p < 0.05, **p < 0.01, ***p < 0.001, ****p < 0.0001.

In a melanoma model, we further investigated the anticancer efficacy of STCs (Figure 2A). As illustrated in Figure 2B–D and Figure S3, both the died STC group and the STC group significantly inhibited tumor growth, while the STC group exhibited a better efficacy. By analyzing intratumoral infiltration of immune cell proportions within the primary tumor, the STC group revealed a more prominent anticancer effect, evidenced by a significant increase of CD4⁺ and CD8⁺ T cells (Figure 2E). Moreover, the ratio of CD8⁺ Granzyme B⁺ and CD8⁺ Ki67⁺ T cell subsets was significantly upregulated in the STC group, significantly higher than that in the died STC group (Figure S4A). A significantly increased proportion of effector memory T cells (TEMs), NK cells, and granzyme B⁺ NK cells in the spleens were also observed in the STC group (Figure 2F and G). These experimental results revealed the efficient activation of the anticancer T cell immunity by both the died STC group and the STC group, while the STC group exhibited better efficacy, possibly due to the prolonged action duration of the live STCs compared to the died STCs.

2.2 Promotion of DCs recruitment by celecoxib

Of note, intratumoral infiltration of DCs following STC treatment did not significantly increase compared to the died STC group (Figure S4B). This could be accounted for that DC recruitment into tumors is typically regulated by NK cells by secreting chemokines such as CCL5 and XCL1 (Böttcher et al., 2018). However, this process can be disrupted by STC-produced PGE2 which inhibits NK cells' activity and production of chemokines (Böttcher et al., 2018; Böttcher and Sousa, 2018). Upregulated COX2 in cellular senescence typically leads to increased PGE2 production (Gorgoulis et al., 2019). Therefore, we proposed the application of liposomal celecoxib (COX2 inhibitor) could reduce PGE2 production and promote DC recruitment.

As shown in Figure 3A, S8, the STCs indeed exhibited higher COX2 expression levels compared to the control cells without senescence. With celecoxib treatment, STCs demonstrated a remarkable decrease in COX2 expression and PGE2 production (Figure 3B–C).

The ability to recruit DCs was evaluated through Transwell experiments after coculturing NK cells with different pretreatment (Figure 3D). STCs activated NK cells more effectively than the Control group, but the amount of migrating DCs recruited by the NK cells was not significantly increased (Figure 3E). By contrast, the NK cells activated by the celecoxib-treated STCs significantly increased the recruitment of DCs (Figure 3E). These results collectively demonstrated that coapplication of celecoxib with STCs enhanced the NK cell activation and DC recruitment efficiency.

2.3 Characterization of STCs+CLX-Lipo@Gel

The preparation of chitosan hydrogel incorporating cells and liposomes was delineated in Figure 4A. Due to the limited solubility of celecoxib in aqueous solutions, we formulated celecoxib liposomes (referred to as CLX-Lipo) for enhanced biocompatibility to the hydrogel matrix. The CLX-Lipo exhibited a spherical morphology with a size of approximately 60 nm and negative zeta potential (Figure 4B–D); the drug encapsulation efficiency was 73.5% and the drug-loading capacity was 2% (Supplementary Table S1).

An injectable, temperature-sensitive chitosan gel was prepared using phosphate buffer (PB) containing sodium bicarbonate (NaHCO₃) as the gelling agent. NaHCO₃ neutralizes the protons of amino groups in chitosan chains, thereby reducing interchain repulsions (Ahmadi and de Bruijn, 2008; Assaad et al., 2015; Monette et al., 2016). By reaching a balance of electrostatic attractions and interchain repulsions, gelation was formed by the entangled chains. An increase in temperature accelerates proton transfer, endowing this hydrogel with temperature-sensitive properties (Ahmadi and de Bruijn, 2008; Assaad et al., 2015; Monette et al., 2016). The gelation times at a temperature of 37°C with varying NaHCO₃ concentrations (0.05 M, 0.075 M, and 0.1 M) were all in 1 h (Figure 4E and Supplementary Table S2). The thus-formed CS@Gel exhibited a reticulated porous structure, with pore size ranging from 5 to 100 μm (Figure 4F). Rheological analysis revealed that the storage modulus (G') of the CS@Gel was significantly higher than the loss modulus (G''), indicating a robust elastic property (Figure 4G). Cell viability

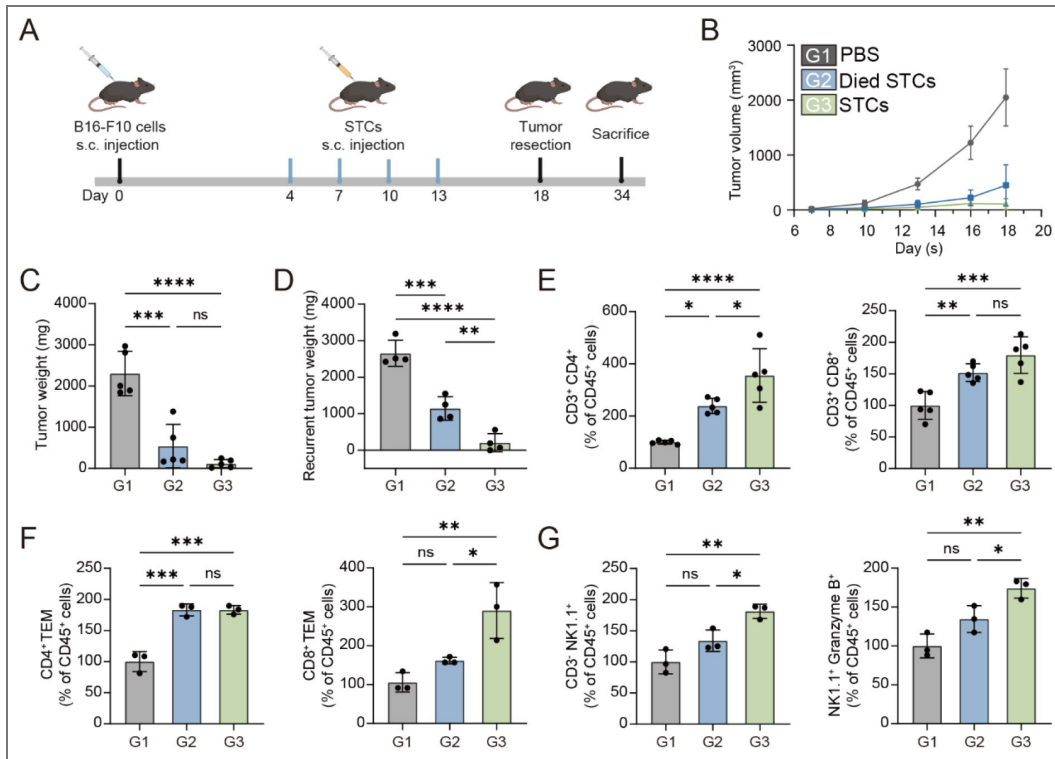


Figure 2. Immunization with senescent B16-F10 cells promoted anticancer immunity.

(A) Schedule of STCs treatment in a recurrent melanoma model. Created with *BioRender.com* <https://www.biorender.com/>. (B) The average tumor volume change of mice treated with different groups (n=5). (C) The tumor weight of the first tumor (n=5). (D) The tumor weight of recurrent tumor (n=4). (E) The percentage of CD3⁺ CD4⁺ and CD3⁺ CD8⁺ T cells within tumors treated with different groups (n=5). (F) The percentage of CD4⁺ and CD8⁺ T cells within spleens of mice treated with different groups (n=3). (G) The percentage of CD3⁺ NK1.1⁺ and NK1.1⁺ Granzyme B⁺ cells within spleens of mice treated with different groups (n=3). Statistical significance was assessed by one-way ANOVA and Tukey multiple comparisons tests. Data were presented as mean ± SD. Statistical significance was determined as *p < 0.05, **p < 0.01, ***p < 0.001, ****p < 0.0001.

Figure 3. Celecoxib promoted the DCs recruitment.

(A–B) COX2 expression in senescent and normal B16-F10 cells with or without celecoxib treatment detected by western blotting and statistical analysis. (C) PGE2 concentrations in the supernatant of different treatments. (D) Schematic diagram of Transwell coculture system. Created with *BioRender.com*. (E) The quantitative analysis of migrated DCs after different treatments. Statistical significance was assessed by one-way ANOVA and Tukey multiple comparisons tests. Data were presented as mean ± SD (n=3). Statistical significance was determined as ns (not significant, p > 0.05), **p < 0.01, ***p < 0.001, ****p < 0.0001.

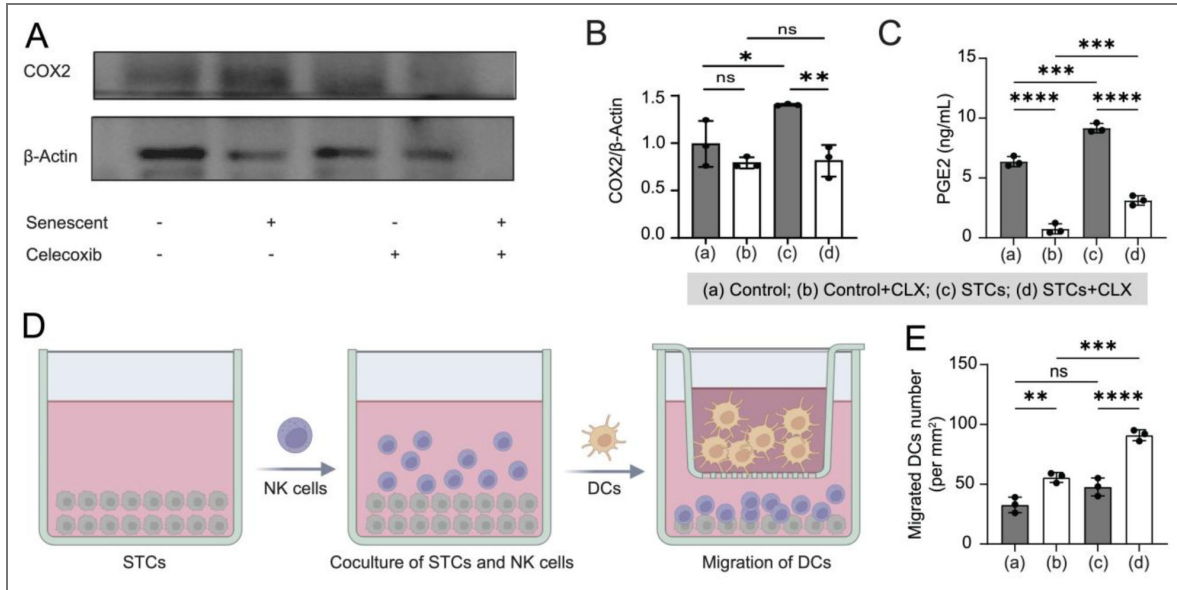
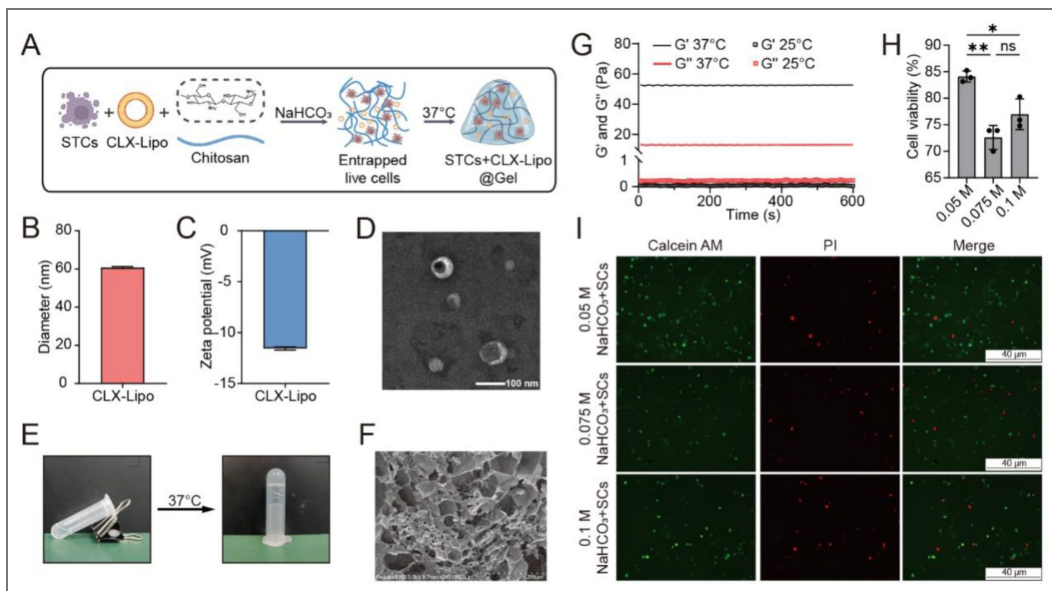


Figure 4. Preparation and characterization of STCs+CLX-Lipo@Gel.

(A) Schematic diagram of the preparation process for STCs+CLX-Lipo@Gel. Created with *BioRender.com*. (B) Particle size and (C) zeta potential of CLX-Lipo. (D) Transmission Electron Microscopy image of CLX-Lipo (scale bar: 100 nm). (E) Photograph of STCs+CLX-Lipo@Gel post-gelatinization. (F) Scanning Electron Microscopy (SEM) image of STCs+CLX-Lipo@Gel. (G) Rheological evaluation of STCs+CLX-Lipo@Gel over time. (H) Quantitative analysis of cell viability for STCs encapsulated within chitosan hydrogel and (I) representative fluorescence images for Live/Dead staining (green: Calcein-AM; red: PI; scale bar: 40 μm). Statistical significance was assessed by one-way ANOVA and Tukey multiple comparisons tests. Data were presented as mean ± SD (n=3). Statistical significance was determined as ns (not significant, p > 0.05), *p < 0.05, **p < 0.01.



remained at 85% after 14 days of culture with the CS@Gel (Figure 4H and I). Given that the 0.05 M group demonstrated the highest cell viability, we employed a NaHCO₃ concentration of 0.05 M to establish the hydrogel system in subsequent experiments.

2.4 DCs and T cells activation by STCs+CLX-Lipo@Gel

We further investigated the synergistic effect of the hydrogel system in activating DCs (Figure 5A). The flow cytometry result showed that the percentage of MHCII⁺ DCs was 82% in the STCs+CLX-Lipo@Gel-treated group, significantly higher than that in the STCs+CLX-Lipo and STCs-treated groups (Figure 5B and C). Conventional type 1 dendritic cells (cDC1) are efficient at presenting exogenous antigens, such as tumor antigens, to CD8⁺ T cells (Böttcher et al., 2018; Böttcher and Sousa, 2018; Ferris et al., 2020). They are pivotal in eliciting cytotoxic effector T-cell responses and orchestrating anti-cancer immune responses (Böttcher and Sousa, 2018). As illustrated in Figure 5D and E, the proportion of cDC1 cells in the PBS group was low (0.3%). After stimulation with STCs, CLX-Lipo-treated STCs, or STC+CLX-Lipo@Gel, the proportion of cDC1 cells in mature DCs was 2.3%, 7.8%, and 14.1%, respectively. These results indicated that STCs+CLX-Lipo@Gel exhibited an improved effect on cDC1 activation, serving as a potent immunoadjuvant.

In a coculture model involving T cells and STCs+CLX-Lipo@Gel, there was a very high count of CD8⁺ T cells, approximately 5.4 times than that of the PBS control group (Figure 5F and G), and there was also a high proportion of Granzyme B⁺ and IFN-γ⁺ CD8⁺ T cells, reaching approximately 45% (Figure 5H and I). In addition, the STCs+CLX-Lipo@Gel treatment also increased the proportion of the proliferative CD8⁺ T cells, consistent with the findings above (Figure 5J and K).

2.5 Restoration of the functionality of the NK-DC axis by STCs+CLX-Lipo@Gel

NKG2D and NKp46, the essential surface receptors on NK cells, can recognize and bind to infected or malignant cells, thereby activating NK cells and facilitating the elimination of target cells (Antonangeli et al., 2016; Kyrysyuk and Wucherpfennig, 2023). We assessed the activation of NK cells through a coculture model (Figure 6A). Compared to the PBS group, both the STC group and the STCs+CLX-Lipo group showed a significant increase in the proportion of NKG2D⁺ and NKp46⁺ NK cells, while the STCs+CLX-Lipo@Gel group exhibited the highest efficacy (Figure 6B and C; Supplementary Figure S5A and B). Besides, coculturing with STCs+CLX-Lipo@Gel resulted in a substantial increase in the proportion of proliferating NK cells (Figure 6D; Supplementary Figure S5C). Consequently, the STCs+CLX-Lipo@Gel treatment markedly enhanced the cytotoxic capacity of NK cells against the tumor cells, as illustrated in Figure 6E.

Notably, inhibition of PGE2 production can reinstall the NK-DC axis and thus promote the recruitment of DCs (Böttcher et al., 2018; Böttcher and Sousa, 2018). Our study revealed that coculture with STCs+CLX-Lipo@Gel led to a marked increase in CCL5 and XCL1 secretion by NK cells (Figure 6F and G), as a result of the significantly reduced levels of PGE2 (Figure 6H). The Transwell assay indicated that the STC group did not promote DC migration, while the STCs+CLX-Lipo@Gel group significantly enhanced DC recruitment, consistent with the aforementioned findings on NK cell chemokine secretion (Figure 6I–J).

2.6 In vivo retention of STCs+CLX-Lipo@Gel

DiR-labeled STCs were utilized to prepare STCs@Gel that were subcutaneously injected into mice to investigate the in vivo retention. As shown in Figure 7A and B, the fluorescence intensity of the STC group gradually diminished after subcutaneous injection, reaching only 1/5 of the initial intensity by the 7th day. By contrast, the STCs@Gel group displayed no substantial decline in fluorescence intensity by the 7th day, with the average fluorescence intensity on the 14th day remaining substantial (Figure 7B). These results indicated that STCs encapsulated within a gel could prolong the in vivo retention of STCs.

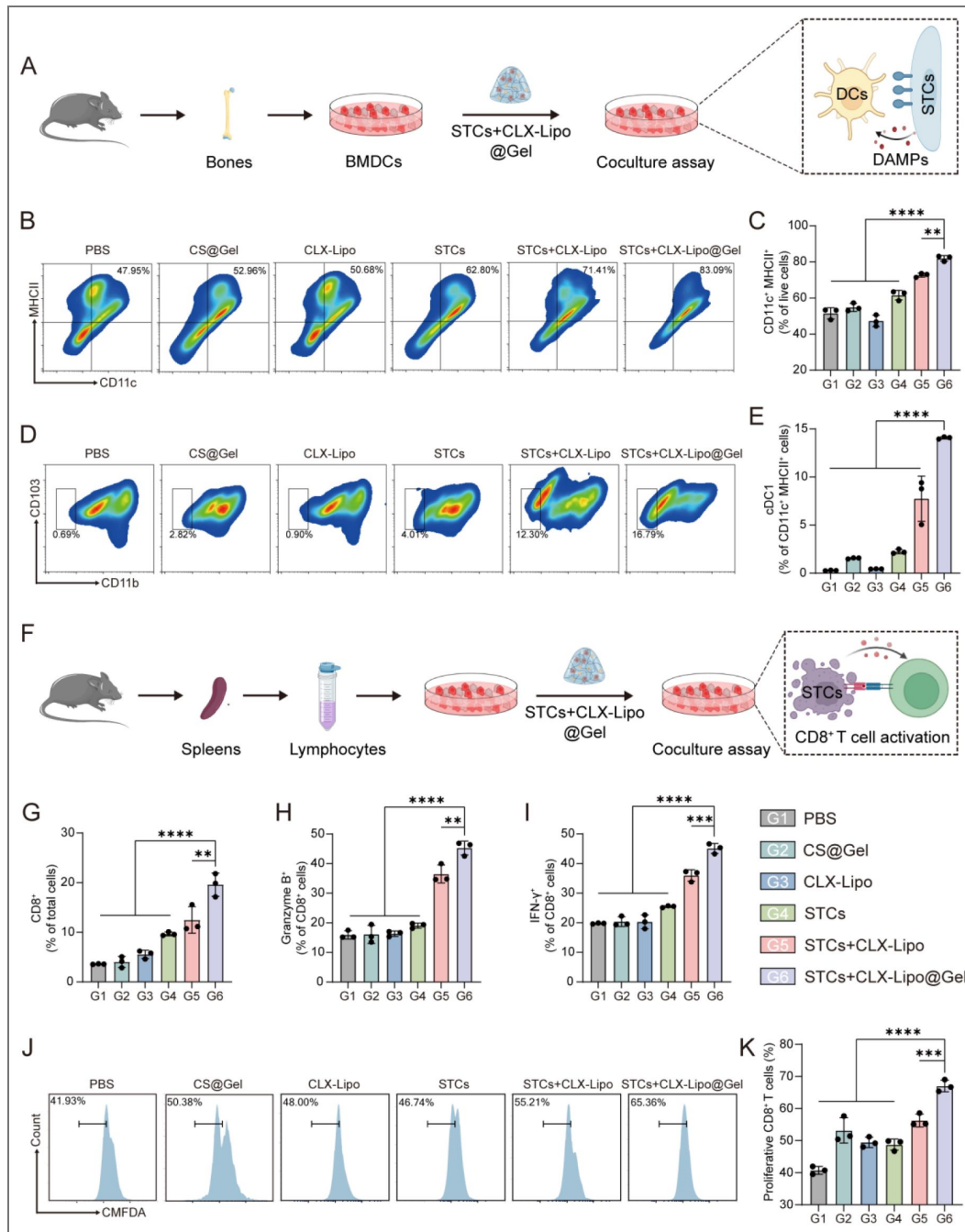
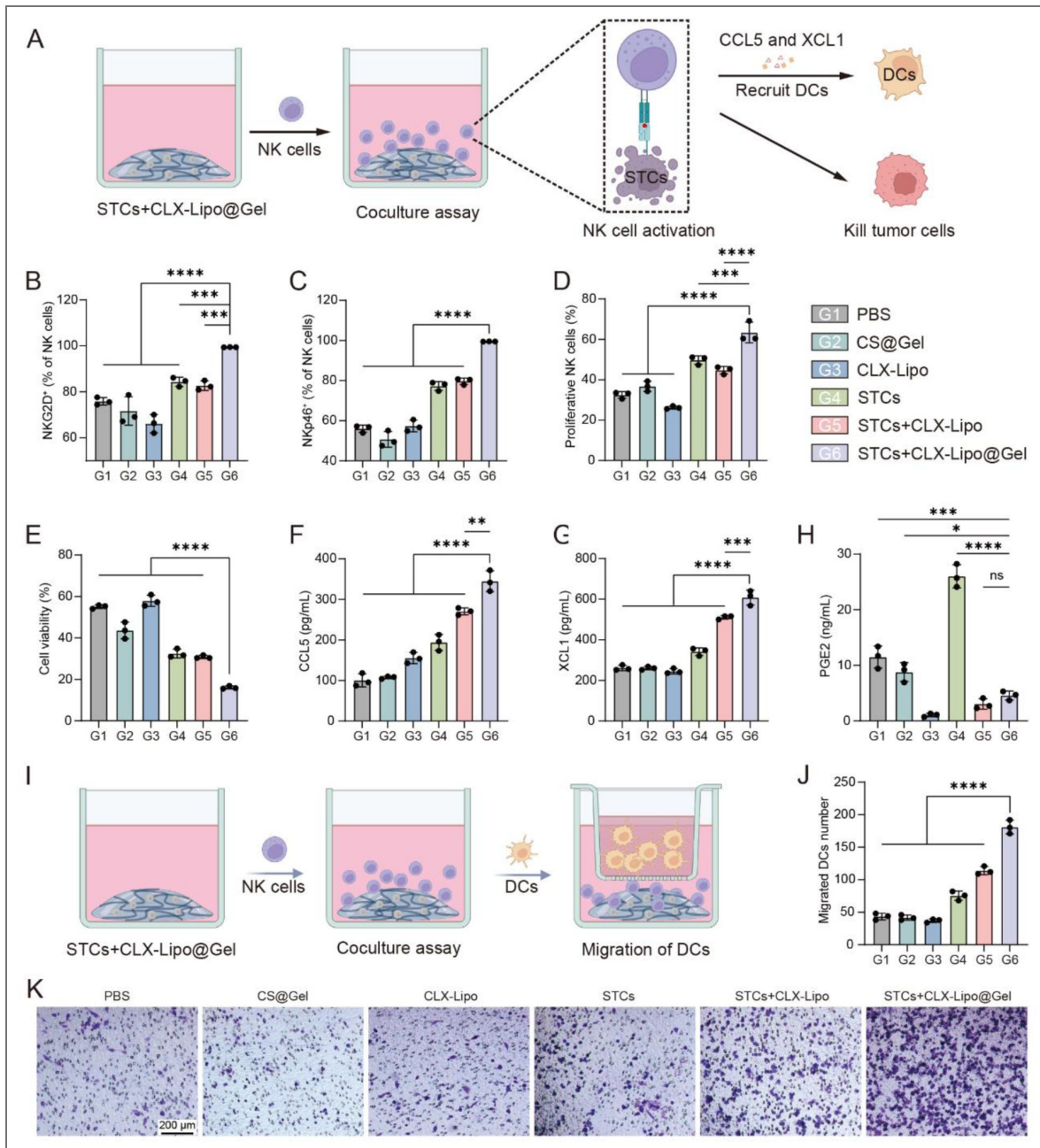


Figure 5. STCs+CLX-Lipo@Gel promoted maturation of DCs and activation of CD8⁺ T cells.

(A) Schematic diagram of coculture of STCs+CLX-Lipo@Gel and BMDCs. (B) Flow cytometry analysis and (C) quantitative analysis of the percentage of CD11c⁺ MHCII⁺ cells after various treatments. (D) Flow cytometry analysis and (E) quantitative analysis of the percentage of cDC1 in matured DCs after various treatments. (F) Schematic diagram of coculture of STCs+CLX-Lipo@Gel and splenic lymphocytes. The percentage of (G) CD8⁺ T cells, (H) Granzyme B⁺ and (I) IFN-γ⁺ in CD8⁺ T cells after various treatments. (J) Flow cytometry histograms depicting CMFDA fluorescence intensity of CD8⁺ cells. (K) Quantitative analysis of the percentage of proliferative CD8⁺ T cells after various treatments. Statistical significance was assessed by one-way ANOVA and Tukey multiple comparisons tests. Data were presented as mean ± SD (n=3). Statistical significance was determined as, **p < 0.01, ***p < 0.001, ****p < 0.0001.



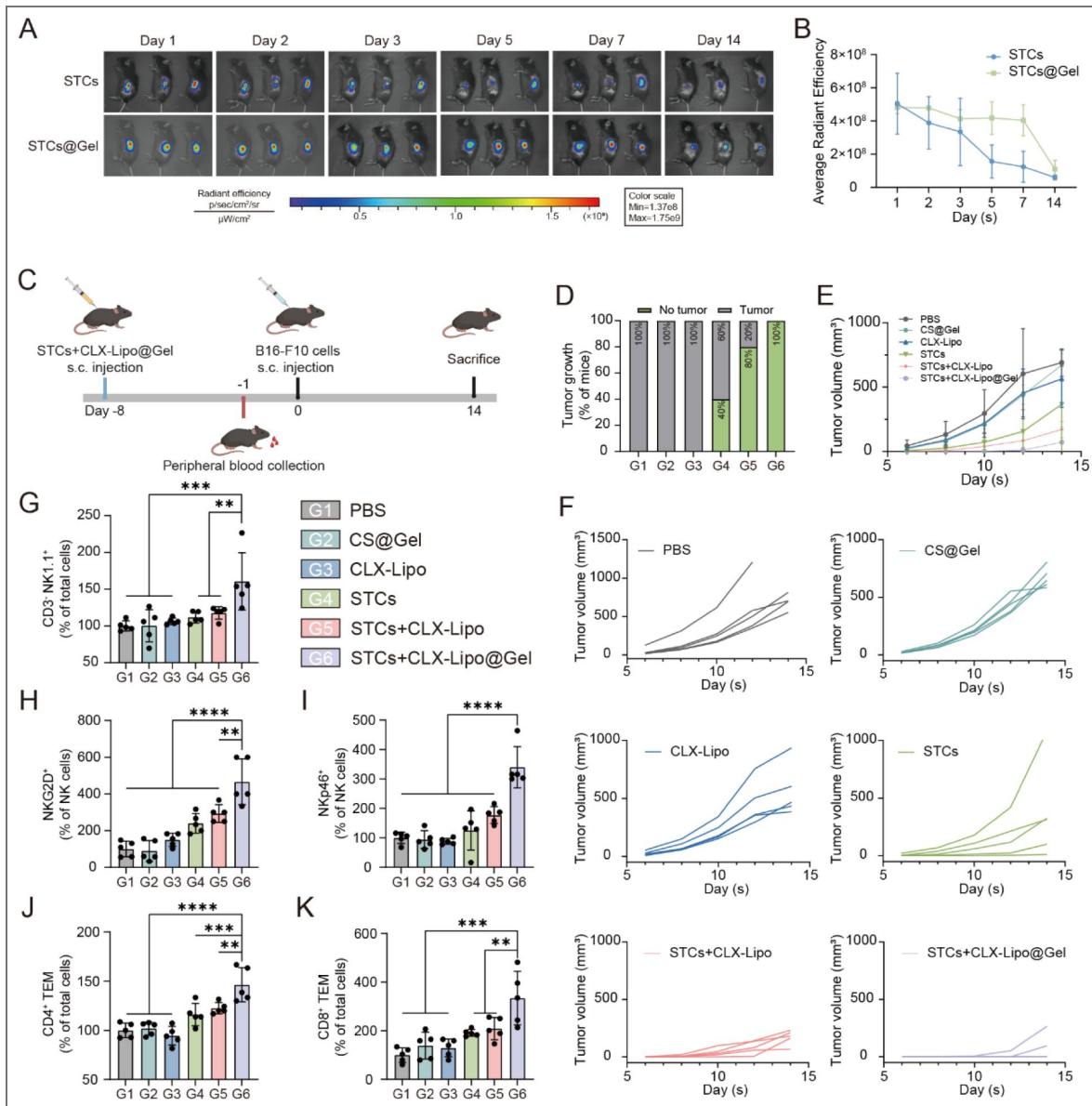


Figure 7. In vivo biodistribution, prophylactic and immunoregulatory effects of STCs+CLX-Lipo@Gel.

(A) Representative IVIS images at different time points of DiR-labeled STCs encapsulated in chitosan hydrogel and (B) semi-quantitative analysis of fluorescent signal ($n=3$). (C) Schedule of various treatments in a melanoma challenge model. Created with *BioRender.com*. (D) Tumor-free rate of different groups on the 7th day. (E) The average tumor growth curve of different groups. (F) The individual tumor growth of each group. (G) The percentage of $CD3^+ NK1.1^+$ cells in peripheral blood after various treatments. The percentage of (H) $NKG2D^+$ and (I) $Nkp46^+$ cells in NK cells in peripheral blood after various treatments. The percentage of (J) $CD4^+$ and (K) $CD8^+$ effector memory T cells (TEMs) in spleens after various treatments. Statistical significance was assessed by one-way ANOVA and Tukey multiple comparisons tests. Data were presented as mean \pm SD ($n=5$). Statistical significance was determined as * $p < 0.05$, ** $p < 0.01$, *** $p < 0.001$, **** $p < 0.0001$.

2.7 In vivo prophylactic efficacy of STCs+CLX-Lipo@Gel

A tumor challenge study was conducted in C57BL/6 mice to evaluate the prophylactic efficacy of the pre-administered STCs+CLX-Lipo@Gel against melanoma development (Figure 7D). By the 7th day, the STCs+CLX-Lipo@Gel group exhibited no observable tumors in any of the mice (Figure 7E), and showed an average tumor volume of only 181 mm³ on the 14th day, and three mice did not develop tumors (Figure 7F and G). By contrast, the tumor growth was rapid in other groups, with an average tumor volume exceeding 500 mm³ by the 14th day (Figure 7F and G).

To evaluate the immune-stimulatory effect of STCs+CLX-Lipo@Gel, we collected the blood and spleen samples for subsequent analysis. Compared to the PBS group, the STCs+CLX-Lipo@Gel group demonstrated a significant increase in both the amount of NK cells and the proportion of activated NK cells (NKG2D⁺ and NKp46⁺) in the blood of mice (Figure 7H–J). Additionally, there was also a significant increase in the proportions of both CD4⁺ TEMs and CD8⁺ TEMs in the spleens of mice receiving STCs+CLX-Lipo@Gel (Figure 7K and L).

2.8 Antitumor effect of STCs+CLX-Lipo@Gel in the subcutaneous melanoma model

The therapeutic efficacy of STCs+CLX-Lipo@Gel was further investigated in a melanoma mouse model (Figure 8A). A single treatment was administered to mice on the 11th day (Figure 8A). As illustrated in Figure 8B and C, the STCs+CLX-Lipo@Gel group exhibited the smallest tumor volume, revealing a significant tumor suppression efficacy (inhibition rate of 94.3%) (Figure 8D and Supplementary Figure S6).

At the experimental endpoint, the lymph nodes and tumor tissues were harvested for flow cytometric analysis of immune cells. The STCs+CLX-Lipo@Gel treatment significantly increased the proportion of mature DCs in the lymph nodes and promoted cDC1 recruitment to the lymph nodes adjacent to the tumors (Figure 8E). The STCs+CLX-Lipo@Gel group also showed a significant increase in the proportion of CD4⁺ and CD8⁺ T cells in the tumor tissue compared to the PBS group (Figure 8F and G). In specific, there was a notable increase in the proportion of the CD8⁺ Ki67⁺ cell subset, suggesting the enhanced proliferation of intratumoral CD8⁺ T cells (Figure 8G). Concurrently, the proportion of CTLs (CD8⁺ Granzyme B⁺) increased significantly in the STCs+CLX-Lipo@Gel group, approximately 5 times higher than that of the PBS group and 2 times higher than that of the STCs+CLX-Lipo group (Figure 8G). Analysis of intratumoral NK cells showed a significant increase in their proportion following treatment with STCs+CLX-Lipo@Gel (Figure 8H). The amount of activated NK cells (NKG2D⁺ and NKp46⁺) also increased significantly, about 2 and 4 times higher than that of the PBS group, respectively (Figure 8H). Accordingly, the proportion of cytotoxic effector NK cells (Granzyme B⁺) also increased significantly (Figure 8H). These results indicated that STCs+CLX-Lipo@Gel treatment could significantly activate anti-tumor immunity.

2.9 Antitumor effect of STCs+CLX-Lipo@Gel in various tumor models

Melanoma brain metastases have emerged as a prevalent and formidable clinical challenge, often culminating in the demise of patients as a direct consequence of the disease (Oliva et al., 2018). We undertook an investigation to ascertain whether this vaccine could mitigate the development of melanoma brain metastases. The mice were vaccinated as depicted in Figure 9A, and the efficacy of the treatment was evaluated through the monitoring of the survival time of the mice bearing intracranial B16F10 tumor. The STCs+CLX-Lipo@Gel treatment exhibited the most extended survival duration, with a median survival time of 16 days, in contrast to 11.5 days for the STCs+CLX-Lipo group and 9 days for the PBS group (Figure 9B and C).

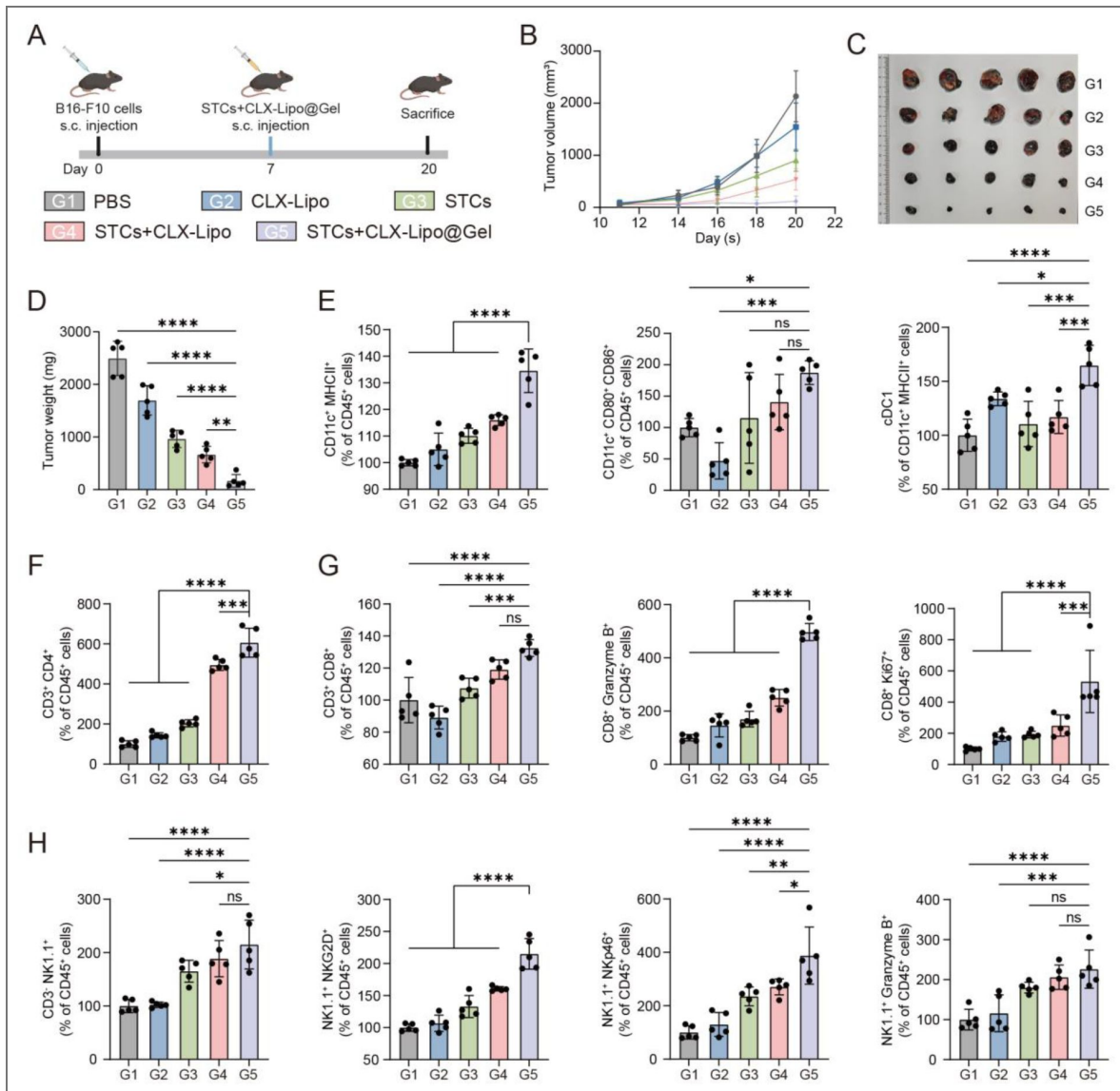


Figure 8. Antitumor and immune-stimulating effects of STCs+CLX-Lipo@Gel in the subcutaneous melanoma model.

(A) Schedule of various treatments in subcutaneous melanoma model. Created with *BioRender.com*. (B) Tumor growth curve, (C) tumor image, and (D) tumor weight of different groups. (E) The percentage of matured DCs (CD11c⁺ MHCII⁺ and CD11c⁺ CD80⁺ CD86⁺) and cDC1 in peritumoral lymph nodes after various treatments. (F) The percentage of CD4⁺ T cells in tumor tissues after various treatments. (G) The percentage of CD8⁺ T cells and activated CD8⁺ T cells (CD8⁺ Granzyme B⁺) proliferative CD8⁺ T cells (CD8⁺ Ki67⁺) in tumor tissues after various treatments. (H) The percentage of NK cells (CD3⁺ NK1.1⁺), and activated NK cells (NK1.1⁺ NKG2D⁺, NK1.1⁺ Nkp46⁺, and NK1.1⁺ Granzyme B⁺) in tumor tissues after various treatments. Statistical significance was assessed by one-way ANOVA and Tukey multiple comparisons tests. Data were presented as mean ± SD (n=5). Statistical significance was determined as *p < 0.05, **p < 0.01, ***p < 0.001, ****p < 0.0001.

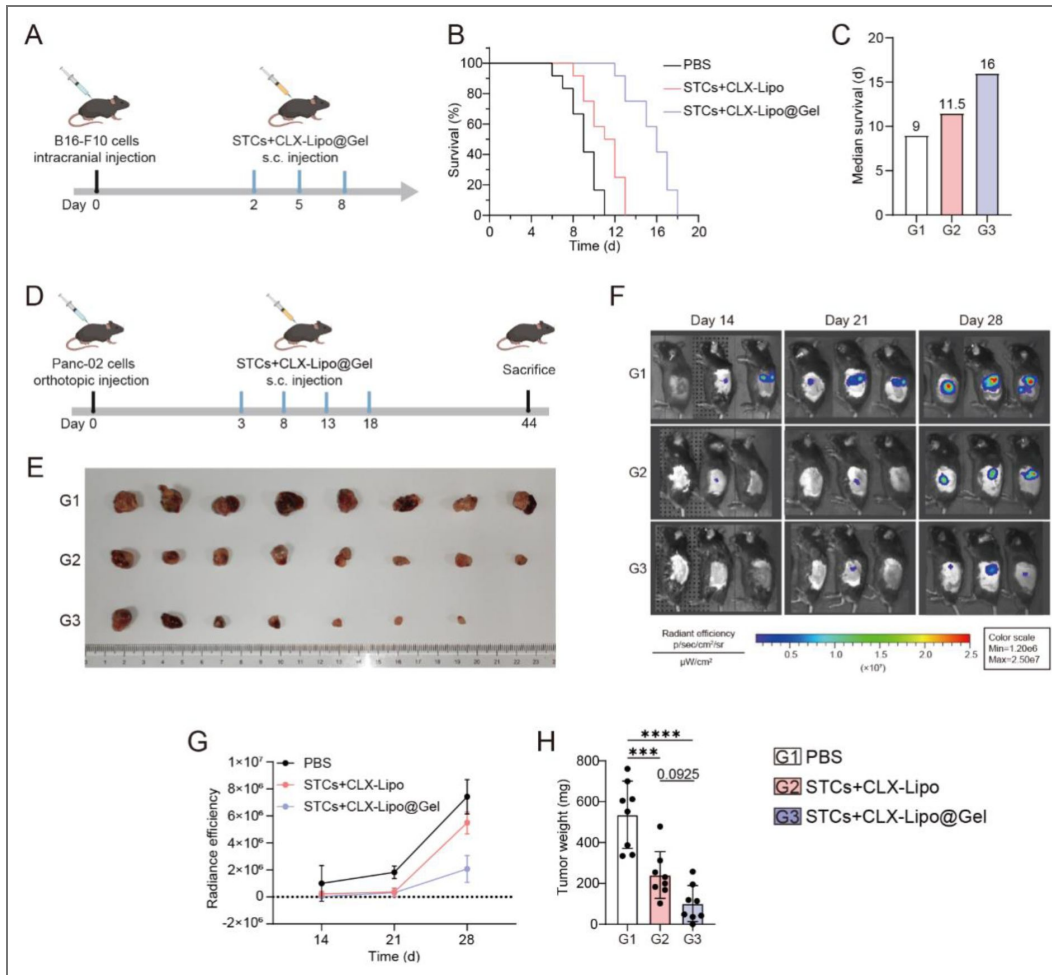


Figure 9. Antitumor effect of STCs+CLX-Lipo@Gel in various tumor models.

(A) Schedule of various treatments in melanoma brain metastasis model. Created with *BioRender.com*. (B) Survival rate and (C) median survival of mice during the treatment period (n=12). (D) Schedule of various treatments in an orthotopic pancreatic cancer model. Created with *BioRender.com*. (E) Tumor image of pancreatic tumors after different treatments (n=8). (F) Representative IVIS images of pancreatic tumors at different time points after different treatments and (G) semi-quantitative analysis of bioluminescence (n=3). (H) Pancreatic tumor weight of different groups (n=8). Statistical significance was assessed by one-way ANOVA and Tukey multiple comparisons tests. Data were presented as mean ± SD. Statistical significance was determined as ***p < 0.001, ****p < 0.0001.

To further explore the general applicability of the live cell vaccine, we conducted a treatment in a typical “cold” tumor model, pancreatic ductal adenocarcinoma (PDAC). In the orthotopic PDAC model, the mice were vaccinated according to the scheme in [Figure 9D](#). The treatment with STCs+CLX-Lipo@Gel showed a significant deceleration in tumor growth ([Figure 9F](#) and [G](#)), with an average tumor weight of merely 101 mg ([Figure 9H](#)). These data underscored the potential of the STCs+CLX-Lipo@Gel as a promising therapeutic strategy, not only in exerting a distant effect on brain metastasis but also in addressing formidable malignancies such as PDAC.

2.10 Biosafety evaluation of STCs+CLX-Lipo@Gel

During the treatment period, a slight increase in body weight was observed in all groups of mice, which initially indicates good biosafety of the formulations ([Supplementary Figure S7A](#)). There were no significant differences in organ coefficients among the groups ([Supplementary Figure S7B](#)), and H&E staining results indicated no significant pathological changes in the main organs in all groups ([Supplementary Figure S7C](#)). Moreover, upon subcutaneous injection, STCs exhibited no tumorigenic capacity ([Supplementary Figure S7D](#)). These experimental results suggested that STCs+CLX-Lipo@Gel had good biosafety.

3 Discussion

Tumor vaccines represent a promising therapeutic strategy. WTC vaccines, containing the complete spectrum of tumor antigens, can elicit robust local innate immune responses and adaptive anti-tumor responses, garnering significant interest from researchers. STCs, with prolonged activity but without proliferation capacity, possess the potential to gradually release tumor antigens and immunostimulatory cytokines, making them a promising candidate as WTC vaccines. SASP plays a dual role in cancer progression ([Faget et al., 2019](#); [Takasugi et al., 2023](#)). In our study, we proposed an SASP regulation method, in which a negative factor PGE2 was inhibited using CLX-Lipo while SASP action was extended for improving anticancer immunity. It suggested that analysis of SASP components and the use of advanced technologies for comprehensive immune regulation holds broad application prospects.

The hydrogel matrix prolonged the action of STCs, and the co-encapsulated CLX-Lipo promoted the recruitment and maturation of DCs by inhibiting PGE2 production. Our *in vivo* studies demonstrated that STCs+CLX-Lipo@Gel significantly enhanced NK cell activation, DC maturation, and cDC1 recruitment, culminating in a marked activation of CD8⁺ T cells in the tumor microenvironment. Notably, STCs+CLX-Lipo@Gel extended the survival of mice with melanoma brain metastases and suppressed tumor growth in mice with orthotopic pancreatic tumors, underscoring its potential as a general immunotherapeutic strategy.

A limitation of this study is that the results do not definitively indicate whether SASP is beneficial or detrimental to anti-tumor effects. However, extrapolations from *in vivo* animal experiments suggest that high-dose application of senescent tumor cells may maximize the potential to activate innate and adaptive immunity, while prolonged presence of these cells could lead to chronic, harmful inflammation and other toxic effects through sustained SASP production. Concentrated application of senescent tumor cells might also expedite the activation of immune surveillance and clearance mechanisms, thereby limiting their survival time in the body and avoiding potential long-term adverse effects.

Additionally, the process of tumor cell senescence generates neoantigens not present in the original tumor cells. The overlap between the antigenic profiles of senescent and original tumor cells, and the impact of these neoantigens on the efficacy of adaptive immune responses against normal tumor cells, remain topics for further investigation through comparative analysis of antigenic profiles.

The results of this study indicate that vaccination strategies based on senescent tumor cells can significantly enhance the anti-tumor efficacy of tumor vaccines, offering new possibilities for the development and clinical application of tumor vaccines. However, given the heterogeneity of tumor cells, the generalizability of the methods developed in this study requires further

exploration. By delving deeper into the interactions between senescent cells and the tumor microenvironment, and clarifying the heterogeneity and commonalities among different tumors, we can provide a basis for the precise application of senescent cells.

4 Conclusion

In summary, our study has elucidated the promising role of senescent tumor cells, with their inherent high immunogenicity and adjuvanticity, in the development of innovative tumor antigen-based vaccines. Through strategic pharmacological interventions targeting the SASP, particularly the inhibition of PGE2 with CLX, we have effectively restored the function of the NK-DC axis. In vivo experiments demonstrated that the combination of STCs with CLX-Lipo in a chitosan hydrogel matrix effectively activated both innate and adaptive immunity, enhancing the infiltration of immune cells within tumors and reconstructing the tumor immune microenvironment. This strategic modulation was pivotal in amplifying the immune-activating properties of WTC vaccines, thereby contributing to the prevention and suppression of melanoma initiation and progression, and achieving remarkable therapeutic efficacy within a cold tumor model of PDAC. Our study demonstrated that employing senescent tumor cells as a basis for tumor vaccine immunotherapy significantly improved the anti-tumor efficacy of these vaccines, providing novel insights for the development and clinical application of tumor vaccines.

5 Material and methods

5.1 Materials

Doxorubicin was purchased from Macklin Biochemical Technology Co., Ltd. (Shanghai, China). Chitosan (Cat. No. 448877) was purchased from Sigma-Aldrich Co., Ltd. (St. Louis, USA). PC-98T, cholesterol, and DSPE-MPEG2000 were obtained from AVT Pharmaceutical Tech Co., Ltd. (Shanghai, China). Total RNA extraction reagent, SYBR green master mix, and CellTracker green CMFDA (5-chloromethyl fluorescein diacetate) were purchased from Yeasen Biotechnology Co., Ltd. (Shanghai, China). Murine granulocyte-macrophage colony-stimulating factor (GM-CSF) and murine interleukin 4 (IL-4) were purchased from Novus Biologicals (Centennial, USA). Senescence β -galactosidase staining kit, red blood cell lysis buffer, BCA protein assay kit, crystal violet staining solution, and second antibodies were supplied from Beyotime Biotech Inc (Haimen, China). Mouse IL-6 and CXCL1/KC ELISA Kit were purchased from Multi Sciences (Lianke) Biotech Co., Ltd. (Hangzhou, China). Celecoxib, cell membrane fluorescence probe DiR, CCK-8 kit, D-luciferin potassium, fetal bovine serum (FBS), and Dulbecco's Modified Eagle's Medium (DMEM) cell culture medium were purchased from Meilun Biotechnology Co., Ltd. (Dalian, China). COX2 (D5H5) XP® Rabbit mAb was purchased from Cell Signaling Technology. β -Actin Rabbit mAb (AC026) was purchased from ABclonal Technology Co., Ltd. (Wuhan, China). Antibodies used for flow cytometry were purchased from BioLegend (San Diego, USA) and BD Biosciences (San Jose, USA).

5.2 Animals

Male C57BL/6 mice (*RRID: MGI:2159769* [↗](#)) aged 6-8 weeks, weighing 18-22 g were obtained from the Shanghai Laboratory Animal Center Co., Ltd. (Shanghai, China), and maintained in an SPF-certified facility with access to sterilized food pellets and distilled water, under a 12-hour light/dark cycle. All the animal experimental procedures were approved by the Institutional Animal Care and Use Committee (IACUC), Shanghai Institute of Materia Medica, Chinese Academy of Sciences (IACUC: 2023-07-HYZ-145).

5.3 Inclusion and Exclusion Criteria for Animal Studies

To ensure consistency and minimize bias in the animal models, the following criteria were applied:

Inclusion criteria: Only healthy male C57BL/6 mice aged 6-8 weeks, weighing 18-22 g, and confirmed free from specific pathogens (as per supplier certification) were included. Mice were acclimatized for at least 7 days prior to experiments, with normal activity levels and no visible

signs of diseases.

Exclusion criteria: Mice exhibiting any abnormalities during acclimatization (e.g., weight loss >10%, lethargy, eating disorders, respiratory distress, or external injuries) were excluded. Tumor-bearing mice were immediately euthanized and excluded from the study if they met any of the following criteria: (1) tumor volume >2000 mm³; (2) any single tumor dimension (length or width) >20 mm. Additionally, mice showing severe distress (e.g., >20% weight loss, immobility, or ulcerated tumors) were euthanized per IACUC guidelines.

5.4 Attrition Management

Attrition (loss of animals due to death, euthanasia, or technical issues) was monitored throughout all experimental phases to ensure data integrity:

In survival studies (e.g., melanoma brain metastases model in [section 5.14.3](#)), any animal death was recorded daily, with cause documented (e.g., tumor burden, procedural complications, or unrelated morbidity). Animals that died or required early euthanasia were included in survival analyses (e.g., Kaplan-Meier curves) until the point of exit, but excluded from endpoint assays (e.g., tumor weight or immune cell analysis) if tissue was unrecoverable. Attrition rates were minimized by adhering to IACUC guidelines.

5.5 Blinding

Treatment administration: All injections were prepared by an independent researcher using coded syringes. Group assignments were concealed from personnel conducting injections and measurements until data analysis.

Tumor assessment: Tumor volume measurements were performed by technicians blinded to treatment groups using anonymized animal IDs.

Survival studies: Endpoint adjudication (death/euthanasia) followed predefined criteria reviewed by two independent blinded investigators.

5.6 Power Analysis

Sample size was based on estimations by power analysis using G*Power ([RRID:SCR_013726](#)) with a level of significance of 0.05 and a power of 0.85.

5.7 Cell culture

The mouse melanoma B16-F10 cell line ([RRID:CVCL_0159](#)) was purchased from Meilun Biotechnology Co., Ltd. (Dalian, China). The natural killer cell line NK-92 ([RRID:CVCL_2142](#)) and NK-92 cell-specific culture medium was purchased from Wuhan Pronucleus Life Science and Technology Co., Ltd. (Wuhan, China). PANC-02/luci cell line ([RRID:CVCL_A8QL](#)) was kindly gifted from Professor Chen Jiang (Fudan University). All cell lines were authenticated by STR profiling tested negative for mycoplasma contamination.

The B16-F10 cells were cultured in DMEM (MA0212, Meilunbio) with 10% FBS (PWL001, Meilunbio), 100 µg/mL of streptomycin and 100 U/mL of penicillin. The NK-92 cells were cultured in an NK-92 cell-specific culture medium (ProCell, China). All the cells were cultured in a humidified incubator set at 37°C and 5% CO₂.

5.8 Senescence induction and characterization

Senescent B16-F10 cells (STCs) were induced by treatment with 200 nM doxorubicin for 2–3 days, followed by cultivation for 5–7 days.

5.8.1 β-galactosidase staining assay

β-galactosidase staining assay was conducted using a senescence β-galactosidase staining kit (Beyotime, C0602) according to the manufacturer's instructions. After incubation, the cells were fixed using β-galactosidase staining fixation solution for 15 min, washed with PBS 3 times, and

stained by β -galactosidase staining working solution at 37°C for 12 h. Then, cells were washed with PBS and visualized by Olympus IX73 inverted microscope.

5.8.2 Gene expression analysis by RT-qPCR

Cell total RNA was extracted according to the protocol provided by the total RNA extraction reagent (Yeasen, 10606ES). The concentration of total RNA in each sample was determined using a microvolume spectrophotometer and subsequently equalized. Reverse transcription was carried out following the instructions of the reverse transcription kit (Yeasen, 11151ES10). Quantitative real-time PCR was conducted using SYBR green master mix (Yeasen, 11201ES08) in the Bio-Rad CFX384 Touch Real-Time PCR Detection System. β -Actin was used as an endogenous control to normalize the relative expression of all target gene mRNAs. The primer sequences are listed in the Supplementary Table S3 [↗](#).

5.8.3 ELISA for measurement of IL-6 and CXCL1

STCs were induced as indicated, and the supernatant was collected and diluted 5-fold with PBS. The concentrations of cytokines were determined according to the instructions provided by the mouse IL-6 ELISA kit (LIANKEBIO, EK206) and mouse CXCL1/KC ELISA kit (LIANKEBIO, EK296).

5.9 In vitro study of STCs

5.9.1 Bone marrow-derived dendritic cells (BMDC) generation

Bone marrow cells were obtained from the femurs and tibias of the C57BL/6 mice. The cells were harvested through centrifugation at 150×g for 5 min and subsequently cultured in RPMI1640 supplemented with 20 ng/ml GM-CSF and 10 ng/ml IL-4. Partial medium replacement was performed every 3 days. On days 6–8, non-adherent and loosely adherent immature dendritic cells were collected.

5.9.2 Assessment of DCs maturation

BMDCs (4×10^5 cells/well) were cocultured with untreated STCs (2×10^5 cells/well) for 48 h. After incubation, DCs were collected and the expression of maturity markers was analyzed using flow cytometry.

Meanwhile, the culture medium was collected to measure ATP and HMGB1 levels. ATP content determination was performed following the instructions of the enhanced ATP assay kit (Meilunbio, MA0440). The standard and sample were added to each well, and the relative light units (RLU) were measured using BioTek Synergy H1 Multi-Mode Microplate Reader. The determination of HMGB1 content was conducted following the instructions provided in the Mouse High Mobility Group Box 1 (HMGB1) ELISA kit.

5.9.3 Assessment of T cells and NK cells activation

The splenic lymphocytes were isolated from healthy C57BL/6 mice according to the protocol provided by the mouse lymphocyte separation medium (DAKEWE, 7211011). The cells (2×10^6 cells/well) were cocultured with untreated and senescent B16-F10 cells for 48 h. Then, the cells were collected to assess the activation of T cells and NK cells using flow cytometry. At the same time, the supernatant from the cell culture was collected and the level of perforin and granzyme B was quantified using the mouse perforin ELISA kit and mouse granzyme B ELISA kit respectively, following the provided instructions.

5.9.4 In vitro DCs recruitment

B16-F10 cells were seeded in 12 well plates and induced senescence as indicated. After celecoxib treatment for 48 h, cells were harvested and the expression of COX2 was assessed using western blot analysis. At the same time, the supernatant from the cell culture was collected and the level of PGE2 was quantified using the Mouse Prostaglandin E2 ELISA Kit, following the provided instructions.

STCs and normal B16-F10 cells were seeded in 12 well plates and treated with celecoxib for 48 hours. Following this, lymphocytes isolated from the spleens of mice were seeded into the wells (2×10^6 /well) and further incubated for an additional 48 hours. Subsequently, BMDCs were seeded into the upper chambers of Transwell inserts with a pore size of $8 \mu\text{m}$ (2×10^5 /well), where they were cocultured with lymphocytes and tumor cells for 48 h. After the completion of the incubation period, the chambers were stained with crystal violet and examined using bright-field microscopy for both counting and photography purposes.

5.10 In vivo immunotherapy effect of STCs

15 male C57BL/6 mice received a subcutaneous injection of 4×10^5 B16-F10 cells in 100 μL PBS on Day 0 and were divided into 3 groups ($n=5$) on Day 4 randomly. Mice were injected with PBS, Died STCs (STCs dealt with freeze-thaw 3 times), and STCs with 2×10^5 cells every 2 days for 4 times. The tumor volume was measured every other day. On Day 18, the tumors were excised completely for subsequent examination. On Day 34, mice were sacrificed, and their tumors and spleens were harvested for subsequent analysis.

To analyze the immune cell population in tumors, tumor tissues were dissected into fragments and enzymatically digested using collagenase IV (1 mg/mL), hyaluronidase (1 mg/mL), and DNase (0.1 mg/mL) at 37 °C for 60 min. The cell suspension was filtered through a 70 μm sieve mesh and stained with primary antibodies of anti-CD45-APC-Cy7 (BD Biosciences Cat# 561586, [RRID:AB_10896305](#)), anti-CD11c-PE-Cy7 (BioLegend Cat# 117318, [RRID:AB_493568](#)), and anti-MHCII-PE (BD Biosciences Cat# 557000, [RRID:AB_396546](#)) for DCs evaluation via flow cytometric analysis. Additionally, to appraise the infiltration of antitumor T lymphocytes, the cell suspension was stained with primary antibodies of anti-CD45-FITC (BioLegend Cat# 372208, [RRID:AB_2687032](#)) (BioLegend Cat# 372208, [RRID:AB_2687032](#)), anti-CD3-PerCP (BioLegend Cat# 100287, [RRID:AB_3683123](#)), anti-CD4-BV605 (BioLegend Cat# 116027, [RRID:AB_2800581](#)), anti-CD8-APC (BioLegend Cat# 100712, [RRID:AB_312751](#)), anti-IFN γ -PE (BioLegend Cat# 505807, [RRID:AB_315401](#)) and anti-Ki67-BV421 (BioLegend Cat# 652411, [RRID:AB_2562663](#)), followed by flow cytometric analysis.

To analyze the immune cell population in the spleen, spleens ($n=3$) were collected and ground to prepare cell suspension. This suspension was then stained with a suite of primary antibodies: anti-CD45-APC-Cy7 (BD Biosciences Cat# 561586, [RRID:AB_10896305](#)), anti-NK1.1-APC (BioLegend Cat# 156505, [RRID:AB_2876525](#)), anti-CD3-BB700 (BD Biosciences Cat# 566494, [RRID:AB_2744393](#)), anti-CD49b-FITC (BioLegend Cat# 103503, [RRID:AB_313026](#)), and anti-Granzyme B-PE (BioLegend Cat# 372208, [RRID:AB_2687032](#)), for the assessment of NK cells. Concurrently, a suite of primary antibodies: anti-CD45-FITC (BioLegend Cat# 372208, [RRID:AB_2687032](#)) (BioLegend Cat# 372208, [RRID:AB_2687032](#)), anti-CD3-BB700 (BD Biosciences Cat# 566494, [RRID:AB_2744393](#)), anti-CD4-BV605 (BioLegend Cat# 116027, [RRID:AB_2800581](#)), anti-CD8-PE (BioLegend Cat# 100708, [RRID:AB_312747](#)), anti-CD44-BB515 (BD Biosciences Cat# 564587, [RRID:AB_2738855](#)), and anti-CD62L-APC (BD Biosciences Cat# 553152, [RRID:AB_398533](#)), was employed for the evaluation of effective memory T cells. These preparations were subjected to flow cytometric analysis to elucidate their immunophenotypes.

5.11 Preparation and characterization of CLX-Lipo

The preparation of celecoxib-loaded liposomes (CLX-Lipo) via the thin-film hydration method involved PC-98T, cholesterol, DSPE-MPEG2000, and celecoxib at the mass ratio of 45/5/2/1, respectively. These components were dissolved in the mixed solvent of chloroform/methanol (2/1, v/v). The solution was subjected to rotary evaporation under a water bath at 42°C until the uniformly dispersed film was formed. Subsequently, it was hydrated with water and sonicated using a 270 W probe for 15 min. The free drug was removed using a G50 Sephadex gel column.

The size and zeta potential of CLX-Lipo were measured by the Zeta Sizer Nanoparticle Analyzer (Malvern, UK). Visualization of CLX-Lipo was achieved by negative staining with 1% uranyl acetate followed by examination using transmission electron microscopy. The encapsulation efficiency

and drug-loading capacity were assessed via high-performance liquid chromatography (HPLC) (1260 Infinity, Agilent Technologies, Palo Alto, USA), and calculated using the following formula:

$$\text{Encapsulation efficiency (\%)} = \frac{\text{Weight of encapsulated drug}}{\text{Weight of drug added}} \times 100\%$$

$$\text{Drug-loading capacity (\%)} = \frac{\text{Weight of encapsulated drug}}{\text{Weight of CLX-Lipo}} \times 100\%$$

5.12 Preparation and characterization of STCs+CLX-Lipo@Gel

The chitosan hydrogel was prepared according to the previously described method. The chitosan solution (3.33%, w/v) was prepared by dissolving chitosan in 0.1 M HCl and sterilized by ultraviolet-light radiation.

The phosphate buffer solution (PB buffer) at pH 8 was prepared by dissolving Na₂HPO₄ and NaH₂PO₄ in a ratio of 1/0.047 (w/w). The gelling agent was prepared by dissolving NaHCO₃ in the PB buffer at a molar ratio of 4:5 (NaHCO₃ to PB buffer). The gelling agent was sterilized by filtration through 0.2 μm filters.

The formulation of the hydrogel incorporating STCs and CLX-Lipo (denoted as STCs+CLX-Lipo@Gel) was achieved via a sequential two-step procedure. Initially, the chitosan solution was amalgamated with the gelling agent (containing PB buffer and NaHCO₃ at double concentration) through a meticulous mixing process executed 15 times via a Luer connector. The entire mixture was then transferred into a single syringe. Subsequently, a syringe containing cell suspension with CLX-Lipo was connected via a Luer connector, and the mixing process was repeated an additional 15 times. The resultant hydrogels were prepared to attain a final concentration of 2% (w/v) chitosan, 0.04 M PB buffer, and 0.05 M NaHCO₃. Control hydrogels were fabricated following the identical protocol without the inclusion of liposomes and cells.

The rheological assessment of chitosan hydrogel was conducted at a constant angular frequency of 1 rad/s and shear strain of 1%. The internal morphology of the chitosan hydrogel was observed using scanning electron microscopy. Briefly, the chitosan hydrogel was rapidly frozen in liquid nitrogen and lyophilized, and at least three random regions were captured to observe its morphology.

5.13 Viability assay of STCs in chitosan hydrogel

The harvested STCs (5×10⁵ cells/mL) were suspended in chitosan hydrogels of varying concentrations, 0.05 M, 0.075 M, and 0.1 M, and subsequently incubated within a 12-well culture plate for 14 days. After culture, a live/dead assay was conducted to evaluate the viability of the cells. 500 μL Calcein AM/PI detection solution was added to each well, followed by incubation of the cells at 37°C in the dark for 30 min. After washing with PBS, the cells were observed under a fluorescence microscope (Olympus IX73, Japan), and images were captured to calculate the proportion of viable cells.

5.14 In vitro study of STCs+CLX-Lipo@Gel

5.14.1 Maturation of BMDCs

Immature BMDCs were cocultured for 48 h with various treatments, including PBS, CS@Gel, CLX-Lipo (5 μM), STCs, STCs+CLX-Lipo (5 μM) and STCs+CLX-Lipo@Gel (5 μM) for 48 h. The cells were stained with primary antibodies of anti-CD11c-FITC (BioLegend Cat# 117306, [RRID:AB_313775](#)), anti-MHCII-PE (BD Biosciences Cat# 557000, [RRID:AB_396546](#)), anti-CD11b-AF647 (BioLegend Cat# 101218, [RRID:AB_389327](#)), and anti-CD103-BV405 (Proteintech Cat# CL405-65047, [RRID:AB_3083818](#)). The cellular subtypes were subsequently analyzed using flow cytometry.

5.14.2 Activation of NK cells

NK-92 cells were plated at a density of 2×10^5 cells per well in a 12-well plate and cocultured with the aforementioned treatments for 48 h. Subsequently, the cells were harvested, and the expression levels of NKp46 and NKG2D on NK cells were assessed using flow cytometry.

To assess the cytotoxicity of NK cells, NK-92 cells were plated at a density of 2×10^5 cells per well in a 12-well plate and cocultured with the aforementioned treatments for 48 h. Subsequently, the NK cells were harvested and cocultured with B16-F10 cells for 18 hours. After co-incubation, the cells were gently rinsed with PBS to eliminate the NK cells. Then, 500 μ L of CCK-8 assay working solution was added to each well, and the plate was further incubated in a cell culture incubator for 2 h. The optical density (OD) was measured at 450 nm, with normal B16-F10 cells used as the control for determining the cell viability rate.

To evaluate the capacity of NK cells to accumulate DCs, NK-92 cells were plated at a density of 2×10^5 cells per well in a 12-well plate and cocultured with the aforementioned treatments for 48 h. Thereafter, freshly prepared BMDCs were seeded into the upper chambers of Transwell inserts with a pore size of 8 μ m (2×10^5 /well) and co-incubated for another 48 h. After the completion of the incubation period, the chambers were subjected to staining with crystal violet and subsequently analyzed via bright-field microscopy for both counting and photography purposes. The supernatant derived from the coculture was subsequently collected and analyzed for the secretion of CCL5, XCL1, and PGE2 using ELISA kits according to the protocols.

5.14.3 Activation of T cells

Lymphocytes extracted from murine spleens were seeded at a density of 1×10^6 cells per well in a 12-well plate and cocultured with the aforementioned treatments for 48 h. The cells were then harvested and stained with primary antibodies of anti-CD3-PerCP-Cy5.5 (BioLegend Cat# 100218, [RRID:AB_1595492](#) (BioLegend Cat# 100218, [RRID:AB_1595492](#))), anti-CD8-BV421 (BioLegend Cat# 100753, [RRID:AB_2562558](#)), anti-Granzyme B-PE (BioLegend Cat# 372208, [RRID:AB_2687032](#)), and anti-IFN γ -APC-Cy7 (BioLegend Cat# 505849, [RRID:AB_2616697](#)). The cellular subtypes were subsequently analyzed using flow cytometry.

5.14.4 Stimulation of T and NK cell proliferation

Lymphocytes harvested from mouse spleens were stained with CMFDA before being seeded at a density of 1×10^6 cells per well in a 12-well plate and cocultured with the aforementioned treatments for 48 h. Following this, the cells were harvested and stained with primary antibodies of anti-CD3-PerCP-Cy5.5 (BioLegend Cat# 100218, [RRID:AB_1595492](#) (BioLegend Cat# 100218, [RRID:AB_1595492](#))), anti-CD8-BV421 (BioLegend Cat# 100753, [RRID:AB_2562558](#)), and anti-NK1.1-APC (BioLegend Cat# 156505, [RRID:AB_2876525](#)). The proportion of proliferating cells was analyzed using cytometry.

5.15 In vivo retention and uptake of STCs in lymph nodes

6 male C57BL/6 mice were divided into 2 groups (n=3). STCs were harvested as described above and incubated with DiR cell membrane fluorescent probe staining solution at 37°C for 30 min. The chitosan hydrogel encapsulating STCs, referred to as STCs@Gel, was according to the previously outlined procedure. Subsequently, STCs suspension and STCs@Gel, which had consistent fluorescence intensity, were subcutaneously injected. The fluorescence intensity was quantified utilizing the IVIS imaging system (Caliper PerkinElmer, Hopkinton, MA, USA) on days 1, 2, 3, 5, 7, and 14, followed by statistical analysis of the obtained data.

5.16 In vivo immunization and immunotherapy study of STCs+CLX-Lipo@Gel

5.16.1 Prophylactic study in melanoma

30 male C57BL/6 mice were divided into 6 groups (n=5) as delineated below: PBS, CS@Gel, CLX-Lipo, STCs, STCs+CLX-Lipo, STCs+CLX-Lipo@Gel. The mice underwent immunization with 2×10^5 STCs, administered subcutaneously, either in the presence or absence of liposomal CLX at a dosage of 2 mg/kg. 7 days after the immunization, the mice were challenged with 1×10^6 B16-F10 cells administered subcutaneously into their left flank. The tumor volumes were recorded every other day. On the 14th day, the mice were euthanized, and tissue samples were procured for subsequent experimental analysis.

On the 7th day following immunization, 200 μ L of blood was collected from the mice's posterior orbital venous plexus. Following erythrocyte lysis, the cells were stained with primary antibodies of anti-CD3-PerCP-Cy5.5 (BioLegend Cat# 100218, *RRID:AB_1595492* [↗](#) (BioLegend Cat# 100218, *RRID:AB_1595492* [↗](#)), anti-NK1.1-APC (BioLegend Cat# 156505, *RRID:AB_2876525* [↗](#)), anti-NKG2D-PE-Dazzle594 (BioLegend Cat# 130213, *RRID:AB_2728147* [↗](#)), and anti-NKp46-BV421 (BioLegend Cat# 137611, *RRID:AB_10915472* [↗](#)). The cellular subtypes were subsequently analyzed via flow cytometry.

On the 14th day following the mice euthanized, spleens were harvested and processed to create a cell suspension through grinding. The cells were stained with primary antibodies of anti-CD3-PerCP-Cy5.5 (BioLegend Cat# 100218, *RRID:AB_1595492* [↗](#) (BioLegend Cat# 100218, *RRID:AB_1595492* [↗](#)), anti-CD4-FITC (BD Biosciences Cat# 553079, *RRID:AB_394609* [↗](#)), anti-CD8-BV421 (BioLegend Cat# 100753, *RRID:AB_2562558* [↗](#)), anti-CD44-PE (BD Biosciences Cat# 553134, *RRID:AB_394649* [↗](#)), and anti-CD62L-APC (BD Biosciences Cat# 553152, *RRID:AB_398533* [↗](#)). The cellular subtypes were subsequently analyzed via flow cytometry.

5.16.2 Immunotherapy study in melanoma

25 male C57BL/6 mice were administered a subcutaneous injection of 4×10^5 B16-F10 cells suspended in 100 μ L PBS on Day 0. These mice were randomly divided into 5 groups (n=5) as follows: PBS, CLX-Lipo, STCs, STCs+CLX-Lipo, STCs+CLX-Lipo@Gel. The dosages administered were consistent with the aforementioned specifications on the 11th day. The tumor volumes were recorded every other day. On the 20th day, the mice were euthanized, and tissue samples were harvested for subsequent experimental analysis.

To analyze the DCs population in lymph nodes, inguinal lymph nodes were collected and grinded to obtain the single-cell suspension. The cells were stained with primary antibodies of anti-CD45-FITC (BioLegend Cat# 372208, *RRID:AB_2687032* [↗](#)), anti-CD11c-PE-Cy7 (BioLegend Cat# 117318, *RRID:AB_493568* [↗](#)), anti-MHCII-PE (BD Biosciences Cat# 557000, *RRID:AB_396546* [↗](#)), anti-CD11b-AF647 (BioLegend Cat# 101218, *RRID:AB_389327* [↗](#)), and anti-CD103-BV405 (Proteintech Cat# CL405-65047, *RRID:AB_3083818* [↗](#)), to facilitate the assessment of DCs via flow cytometric analysis.

To analyze the immune cell population in tumors, the cell suspension was obtained as mentioned above. The cell suspension was stained with primary antibodies of anti-CD45-FITC (BioLegend Cat# 372208, *RRID:AB_2687032* [↗](#)), anti-CD3-PerCP-Cy5.5 (BioLegend Cat# 100218, *RRID:AB_1595492* [↗](#)), anti-NK1.1-APC (BioLegend Cat# 156505, *RRID:AB_2876525* [↗](#)), anti-NKG2D-PE-Dazzle594 (BioLegend Cat# 130213, *RRID:AB_2728147* [↗](#)), and anti-NKp46-BV421 (BioLegend Cat# 137611, *RRID:AB_10915472* [↗](#)) for NK cells evaluation via flow cytometric analysis. Additionally, to evaluate the infiltration of antitumor T lymphocytes, the cell suspension was stained with primary antibodies of anti-CD45-FITC (BioLegend Cat# 372208, *RRID:AB_2687032* [↗](#)), anti-CD3-PerCP (BioLegend Cat# 100287, *RRID:AB_3683123* [↗](#)), anti-CD8-BV421 (BioLegend Cat# 100753, *RRID:AB_2562558* [↗](#)), anti-IFN γ -PE-Cy7 (BioLegend Cat# 505825, *RRID:AB_1595591* [↗](#)), anti-Granzyme B-PE (BioLegend Cat# 372208, *RRID:AB_2687032* [↗](#)), and anti-Ki67-APC (BioLegend Cat# 652405, *RRID:AB_2561929* [↗](#)), followed by flow cytometric analysis.

5.16.3 Therapeutic efficacy in melanoma brain metastases model

Mice models for melanoma brain metastases were established through intracranial injections of 5×10^3 B16-F10 cells in 5 μ L of PBS into the striatum, located 2 mm right lateral to the bregma, of male C57BL/6 mice. These mice were randomly divided into 3 groups as follows: PBS, STCs+CLX-Lipo, STCs+CLX-Lipo@Gel. Each mouse received subcutaneous immunizations with 5×10^5 STCs and liposomal CLX at a dosage of 2 mg/kg on days 3, 6, and 9. In the survival study, the survival rate was recorded (n=10).

5.16.4 Therapeutic efficacy in orthotopic pancreatic ductal adenocarcinoma model

Senescent PANC-02 cells were induced by treatment with 200 nM doxorubicin for 2 days, followed by cultivation for 5–7 days. The orthotopic PANC-02 PDAC model was established by injecting 2×10^6 PANC-02/luci cells suspended in 50 μ L matrigel directly into the pancreas of male C57BL/6 mice. The mice were randomly divided into 3 groups as follows: PBS, STCs+CLX-Lipo, STCs+CLX-Lipo@Gel. Each mouse received subcutaneous immunizations with 5×10^5 STCs and liposomal CLX at a dosage of 2 mg/kg on days 3, 7, 11, and 15. D-luciferin potassium solution was administered intraperitoneally at a dose of 150 mg/kg. Bioluminescence was then detected using the IVIS Spectrum imaging system, 10 minutes after injection, every 7 days. On day 46 post-tumor inoculation, the mice were euthanized, and the tumors were harvested for further analysis.

5.17 Biosafety evaluation

The body weight of the mice was measured during the treatment. After the end of the experiment, the hearts, livers, spleens, lungs, and kidneys of the mice were harvested. After being thoroughly washed with PBS and excess liquid absorbed with filter paper, they were weighed and recorded to calculate the organ coefficients.

$$\text{Organ Coefficient} = \frac{\text{Organ Mass}}{\text{Mouse Body Weight}}$$

The organ tissues were then immersed in a 4% paraformaldehyde solution for fixation and stored at 4°C. The samples underwent paraffin embedding, tissue sectioning, and H&E staining. Pathological sections were scanned using a pathology slide scanner to assess pathological changes in the organs of mice from different groups, providing a preliminary evaluation of safety.

In the tumorigenesis experiment, 12 male C57BL/6 mice were randomly segregated into three groups, each receiving a subcutaneous injection of 1×10^6 , 2×10^6 , and 5×10^6 B16-F10 cells suspended in 100 μ L PBS respectively, with subsequent monitoring for tumor development.

5.18 Statistical analysis

All data analysis in this study was performed using GraphPad Prism 9.0 software (RRID:SCR_002798 https://doi.org/10.1093/RRID/SCR_002798). The data were presented as mean \pm standard deviation. For multiple groups (three or more), statistical analysis was performed using one-way analysis of variance (ANOVA); for two groups, a t-test was employed. Statistical significance was determined as *p < 0.05, **p < 0.01, ***p < 0.001, ****p < 0.0001.

Supporting Information

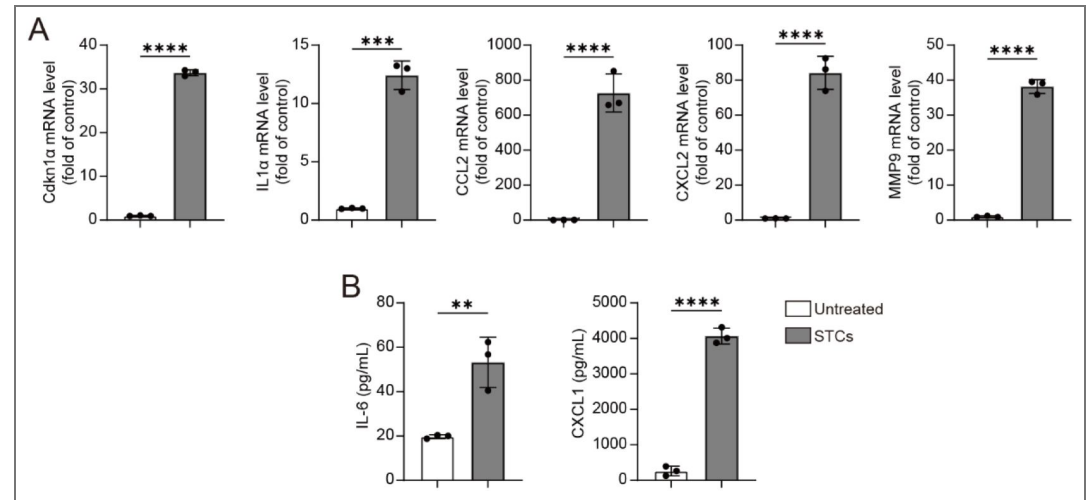


Figure S1. Senescent B16-F10 cells characterization. (A) mRNA expression levels of Cdkn1a, IL1a, CCL2, CXCL2, and MMP9 of senescent B16-F10 cells; (B) The concentrations of IL-6 and CXCL1 in the supernatant of senescent B16-F10 cells. Statistical significance was assessed by unpaired Student's t-test. Data were presented as mean \pm SD. Statistical significance was determined as ** $p < 0.01$, *** $p < 0.001$, **** $p < 0.0001$.

Figure S2. Alterations in immune-related cytokines and NK cell-activated receptor ligands at the gene expression level.

(A) mRNA expression levels of chemokines CCL2 and CCL5 in STCs; (B) mRNA expression levels of NKG2D ligands ULBP-1 and RAE-1, and DNAM-1 ligand CD155 in STCs; (C) mRNA expression levels of immune-related cytokines IFN- γ , IL-2, IL-12, and IL-15. Statistical significance was assessed by unpaired Student's t-test. Data were presented as mean \pm SD. Statistical significance was determined as * $p < 0.05$, ** $p < 0.01$, *** $p < 0.001$, **** $p < 0.0001$.

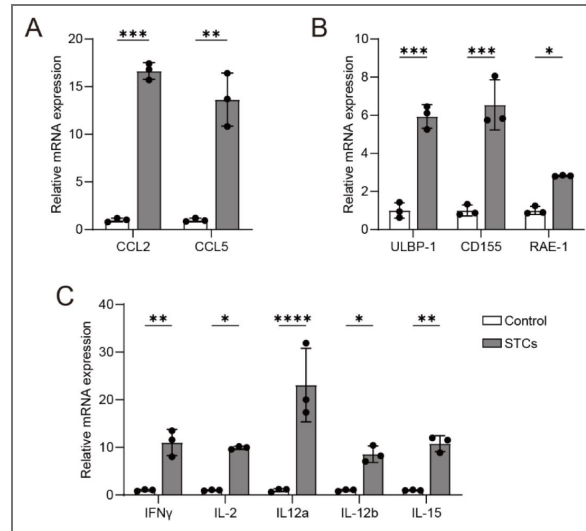


Figure S3. Tumor image of the first tumor (n=5).

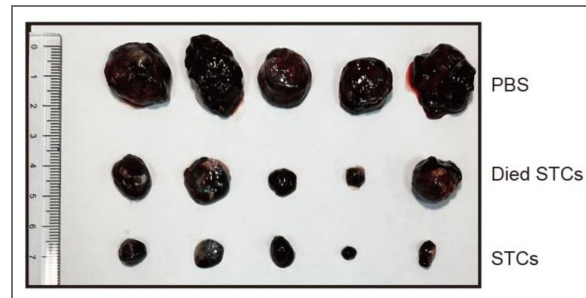


Figure S4. The percentage of (A) activated CD8⁺ T cells (CD8⁺ Granzyme B⁺), proliferative CD8⁺ T cells (CD8⁺ Ki67⁺), (B) matured DCs (CD11c⁺ MHCII⁺ and CD11c⁺ CD80⁺ CD86⁺) in tumor tissues after different treatments.

Statistical significance was assessed by one-way ANOVA and Tukey multiple comparisons tests. Data were presented as mean \pm SD. Statistical significance was determined as ns (not significant, $p > 0.05$), * $p < 0.05$, ** $p < 0.01$, *** $p < 0.001$, **** $p < 0.0001$.

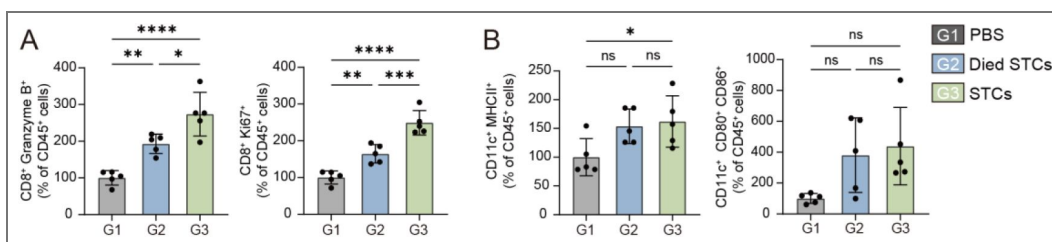


Figure S5. Flow cytometry histograms illustrating fluorescence intensity of (A) NKG2D⁺, (B) NKp46⁺, and (C) proliferative NK cells.

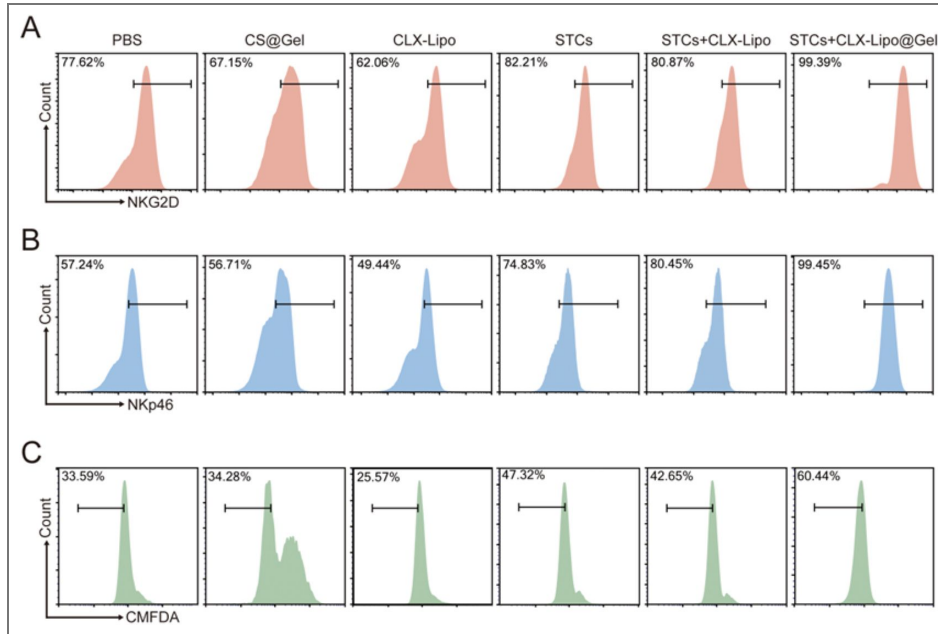
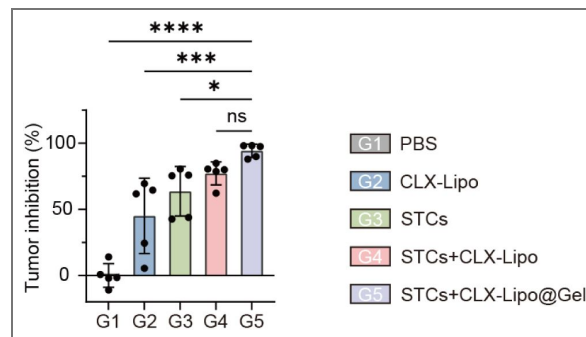


Figure S6. Tumor inhibition rate of different groups.

Statistical significance was assessed by one-way ANOVA and Tukey multiple comparisons tests. Data were presented as mean \pm SD. Statistical significance was determined as ns (not significant, $p > 0.05$), * $p < 0.05$, ** $p < 0.01$, *** $p < 0.001$, **** $p < 0.0001$.



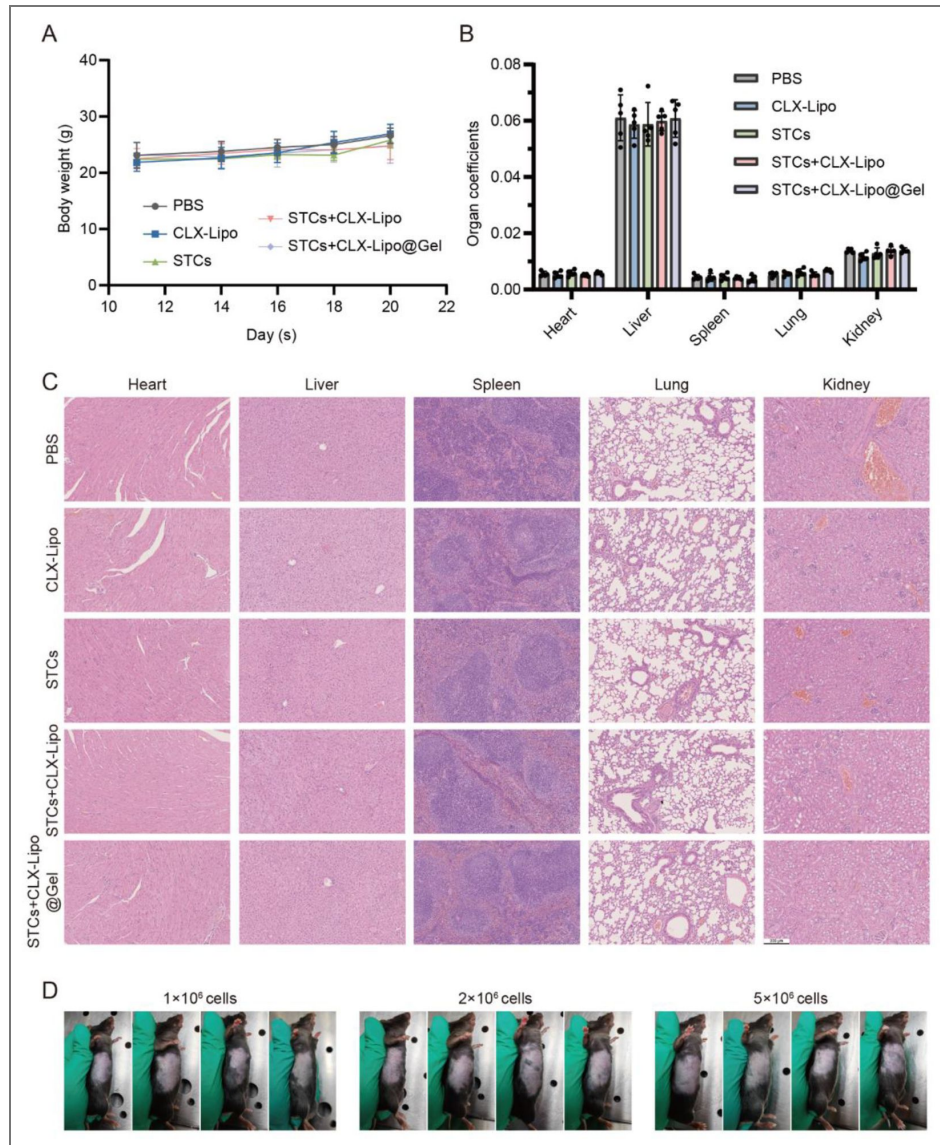


Figure S7. Biosafety evaluation of STCs+CLX-Lipo@Gel.

(A) Body weight changes during different treatments; (B) Organ coefficients after different treatments; (C) Histological examination of the major organs in each group; (D) Tumorigenic potential of senescent B16-F10 cells. Imaging was conducted on the 42nd day post-subcutaneous administration of varying quantities of senescent B16-F10 cells. Data were presented as mean \pm SD (n=5).

Figure S8. Raw data of western blots in Figure 3A.

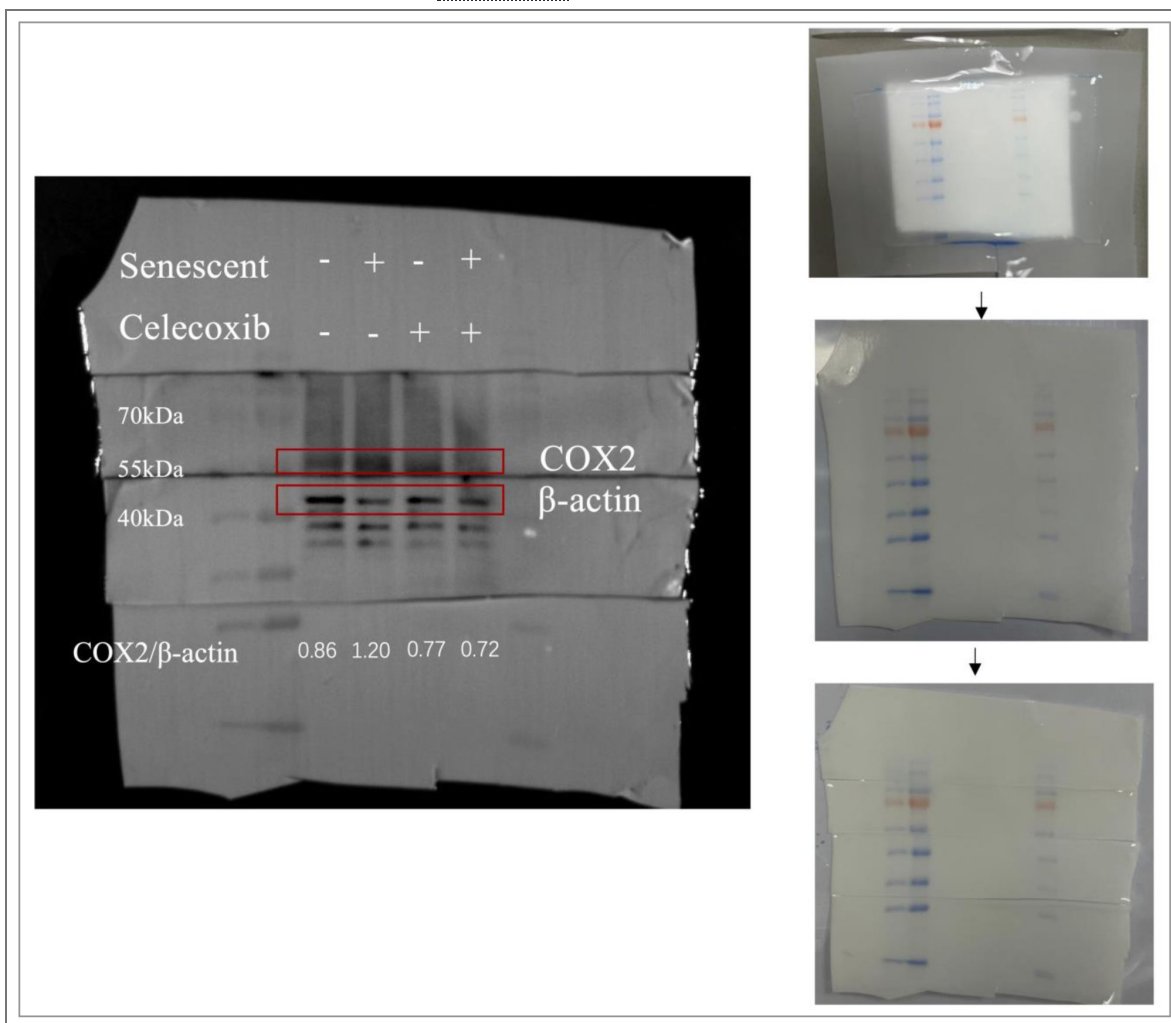


Table S1. Drug encapsulation efficiency and drug-loading capacity of CLX-Lipo.

Encapsulation efficiency	Loading capacity (%)
73.49 \pm 1.66	2.00 \pm 0.04

Table S2. The gelation time of CS@Gel at different concentrations of gelating agent.

NaHCO ₃ (M)	PB (M)	Gelation time (min)
0.05		10
0.075	0.04	12
0.1		45

Table S3. Primer sequences for qPCR analysis.

Gene	Forward Primer (5' to 3')	Reverse Primer (5' to 3')
<i>Cdkn1a</i>	ATCACCAGGATTGGACATG G	CGGTGTCAGAGTCTAGGGGA
<i>CCL2</i>	ACTGAAGCCAGCTCTCTCTT CCTC	TTCCTTCTTGGGGTCAGCACA GAC
<i>CXCL2</i>	TCCAGAGCTTGAGTGTGACG	TCAGTTAGCCTTGCCTTTGTTC
<i>IL-1α</i>	CGCTTGAGTCGGCAAAGAA AT	TGGCAGAACTGTAGTCTTCGT
<i>MMP9</i>	TCAGGGAGATGCCCATTTTCG	GAACGGGAACACACAGGGTT TG
<i>IL-2</i>	TCCTCACAGTGACCTCAAGT CC	TGACAGAAGGCTATCCATCTC C
<i>IL-12a</i>	ACGCACTTGTCTTGAGATG	CTGACCTTGGGAGACACATTT
<i>IL-12b</i> <i>ULBP1</i>	TGGGACCTTGGGGTAATGCT GTTTGGTAAAGAGGGGAGG GG	CAGGTGTGGTTGGGCTTCAC AGAAAGGGGCACTAGAAGTT GC
<i>IL-15</i>	TGCAGCGCGTAAGGAGATG	CGCTCCTTGTGCCTTGATTG
<i>IFN-γ</i>	AATCAAGCTGCCTCCCGTAT	CCTGCTTCACCTCCTAGCTTT
<i>RAE1</i>	CTCTGGAGCCAAAAGTCTGA GT	GACTGGCAAGCAGTGGTGTA
<i>CD155</i>	ACGCAGGCATAAGACGACA A	ATGAGGTAGGAGGGTTGCCT
<i>CCL2</i>	ACTGAAGCCAGCTCTCTCTT CCTC	TTCCTTCTTGGGGTCAGCACA GAC
<i>CCL5</i>	TGCTGGGCTCTTTACACGAT	TTATGGAGCTTCGGCTTGGG
<i>β-Actin</i>	CGGTTCCGATGCCCTGAGGC TCTT	CGTCACACTTCATGATGGAAT TGA

Data availability

All data generated or analyzed during this study are included in the manuscript and supporting files

Acknowledgements

We thank the staff members of the Large-scale Protein Preparation System at the National Facility for Protein Science in Shanghai (NFPS), Shanghai Advanced Research Institute, Chinese Academy of Science, for providing technical support and assistance in data collection and analysis. Special thanks are to Prof. Chen Jiang at Fudan University for providing the PANC02/luci cell lines.

Additional information

Funding

We are thankful for the support from the National Key Research and Development Program of China (2024YFA1210200, 2022YFE0203060), NSFC (82341232, China), the Future Network (083GJHZ2023012FN) and Grand Challenges (083GJHZ2023021GC) of the International Partnership Program of the Chinese Academy of Sciences, CAS President's International Fellowship Initiative (2024VBB0004), and High-level Innovative Research Institute (2021B0909050003) from Department of Science and Technology of Guangdong Province, and Zhongshan Municipal Bureau of Science and Technology (LJ2021001 & CXTD2022011).

Author Contributions

Yuewei Wang: conceptualization, methodology, investigation, formal analysis, data curation, and writing – original draft.

Ante Ou: methodology, investigation, and writing – review and editing.

Yanli Luo: investigation and writing – review and editing.

Yanrong Gao: methodology and investigation.

Yi Zhang: methodology and investigation.

Linxi Qin: investigation.

Yongzhuo Huang*: conceptualization, methodology, writing – review and editing, supervision, and funding acquisition.

Ethics statement

All the animal experimental procedures were approved by the Institutional Animal Care and Use Committee (IACUC), Shanghai Institute of Materia Medica, Chinese Academy of Sciences (IACUC: 2023-07-HYZ-145).

During the preparation of this work the authors used an AI tool (Deepseek V3.1) to improve readability and language of this manuscript. After using this tool, the authors reviewed and edited the content as needed and take full responsibility for the content of the publication.

Abbreviations

cDC1: Conventional type 1 dendritic cells
CLX: Celecoxib
DAMPs: Damage-associated molecular patterns
DCs: Dendritic cells
DMEM: Dulbecco's Modified Eagle's Medium
FBS: Fetal bovine serum
HMGB1: High mobility group box-1 protein
HPLC: High-performance liquid chromatography

NK: Natural killer
 PB: Phosphate buffer
 PDAC: Pancreatic ductal adenocarcinoma
 PGE2: Prostaglandin E2
 SA β G: Senescence-associated β -galactosidase
 SASP: Senescence-associated secretory phenotype
 STCs: Senescent tumor cells
 SEM: Scanning electron microscope
 TAAs: Tumor-associated antigens
 TSAs: Tumor-specific antigens
 TEMs: Effector memory T cells
 WB: Western blot
 WTC: Whole tumor cell

Funding

Funder	Grant reference number	Author
National Natural Science Foundation of China	82341232	Yongzhuo Huang
MOST National Key Research and Development Program of China (NKPs)	2024YFA1210200	Yongzhuo Huang

Author ORCID iDs

Yongzhuo Huang: <https://orcid.org/0000-0001-7067-8915>

References

- Ahmadi R., de Bruijn J.D. (2008) Biocompatibility and gelation of chitosan-glycerol phosphate hydrogels. *J Biomed Mater Res A* **86a**:824-832
- Antonangeli F., Soriani A., Ricci B., Ponzetta A., Benigni G., Morrone S., Bernardini G., Santoni A. (2016) Natural killer cell recognition of drug-induced senescent multiple myeloma cells. *Oncoimmunology* **5**
- Antonangeli F., Zingoni A., Soriani A., Santoni A. (2019) Senescent cells: Living or dying is a matter of NK cells. *J Leukocyte Biol* **105**:1275-1283
- Assaad E., Maire M., Lerouge S. (2015) Injectable thermosensitive chitosan hydrogels with controlled gelation kinetics and enhanced mechanical resistance. *Carbohydr Polym* **130**:87-96
- Bluth M.J., Zaba L.C., Moussai D., Suárez-Fariñas M., Kaporis H., Fan L., Pierson K.C., White T.R., Pitts-Kiefer A., Fuentes-Duculan J., *et al.* (2009) Myeloid Dendritic Cells from Human Cutaneous Squamous Cell Carcinoma Are Poor Stimulators of T-Cell Proliferation. *J Invest Dermatol* **129**:2451-2462
- Böttcher J.P., Bonavita E., Chakravarty P., Blees H., Cabeza-Cabrerizo M., Sammicheli S., Rogers N.C., Sahai E., Zelenay S., Sousa C.R.E. (2018) NK Cells Stimulate Recruitment of cDC1 into the Tumor Microenvironment Promoting Cancer Immune Control. *Cell* **172**:1022
- Böttcher J.P., Sousa C.R.E. (2018) The Role of Type 1 Conventional Dendritic Cells in Cancer Immunity. *Trends in Cancer* **4**:784-792
- Chen H.A., Ho Y.J., Mezzadra R., Adrover J.M., Smolkin R., Zhu C.Y., Woess K., Bernstein N., Schmitt G., Fong L., *et al.* (2023) Senescence Rewires Microenvironment Sensing to Facilitate Antitumor Immunity. *Cancer Discovery* **13**:432-453
- Deng J.J., Xu W.D., Lei S.Y., Li W.Y., Li Q.H., Li K.Q., Lyu J.X., Wang J.L., Wang Z. (2022) Activated Natural Killer Cells-Dependent Dendritic Cells Recruitment and Maturation by Responsive Nanogels for Targeting Pancreatic Cancer Immunotherapy. *Small* **18**
- Faget D.V., Ren Q.H., Stewart S.A. (2019) Unmasking senescence: context-dependent effects of SASP in cancer. *Nature Reviews Cancer* **19**:439-453

- Ferris S.T., Durai V., Wu R., Theisen D.J., Ward J.P., Bern M.D., Davidson J.T., Bagadia P., Liu T.T., Briseño C.G., *et al.* (2020) cDC1 prime and are licensed by CD4⁺ T cells to induce anti-tumour immunity. *Nature* **584**:624
- Gasek N.S., Kuchel G.A., Kirkland J.L., Xu M. (2021) Strategies for targeting senescent cells in human disease. *Nature Aging* **1**:870-879
- Gorgoulis V., Adams P.D., Alimonti A., Bennett D.C., Bischof O., Bishop C., Campisi J., Collado M., Evangelou K., Ferbeyre G., *et al.* (2019) Cellular Senescence: Defining a Path Forward. *Cell* **179**:813-827
- Hasegawa T., Oka T., Son H.G., Oliver-García V.S., Azin M., Eisenhaure T.M., Lieb D.J., Hacoheh N., Demehri S. (2023) Cytotoxic CD4⁺ T cells eliminate senescent cells by targeting cytomegalovirus antigen. *Cell* **186**:1417
- Iannello A., Thompson T.W., Ardolino M., Lowe S.W., Raulet D.H. (2013) p53-dependent chemokine production by senescent tumor cells supports NKG2D-dependent tumor elimination by natural killer cells. *J Exp Med* **210**:2057-2069
- Jahani V., Yazdani M., Badiie A., Jaafari M.R., Arabi L. (2023) Liposomal celecoxib combined with dendritic cell therapy enhances antitumor efficacy in melanoma. *Journal of Controlled Release* **354**:453-464
- Krysyuk O., Wucherpennig K.W. (2023) Designing Cancer Immunotherapies That Engage T Cells and NK Cells. *Annu Rev Immunol* **41**:17-38
- Lee S., Schmitt C.A. (2019) The dynamic nature of senescence in cancer. *Nat Cell Biol* **21**:94-101
- Liu Y., Pagacz J., Wolfgeher D.J., Bromerg K.D., Gorman J.V., Kron S.J. (2023) Senescent cancer cell vaccines induce cytotoxic T cell responses targeting primary tumors and disseminated tumor cells. *J Immunother Cancer* **11**
- Marin I., Boix O., Garcia-Garjón A., Sirois I., Caballe A., Zarzuela E., Ruano I., Attolini C.S.O., Prats N., López-Domínguez J.A., *et al.* (2023a) Cellular Senescence Is Immunogenic and Promotes Antitumor Immunity. *Cancer Discovery* **13**:410-431
- Marin I., Serrano M., Pietrocola F. (2023b) Recent insights into the crosstalk between senescent cells and CD8 T lymphocytes. *npj Aging* **9**
- Meng Y., Efimova E.V., Hamzeh K.W., Darga T.E., Mauceri H.J., Fu Y.-X., Kron S.J., Weichselbaum R.R. (2012) Radiation-inducible Immunotherapy for Cancer: Senescent Tumor Cells as a Cancer Vaccine. *Molecular Therapy* **20**:1046-1055
- Monette A., Ceccaldi C., Assaad E., Lerouge S., Lapointe R. (2016) Chitosan thermogels for local expansion and delivery of tumor-specific T lymphocytes towards enhanced cancer immunotherapies. *Biomaterials* **75**:237-249
- Oliva I.C.G., Schvartsman G., Tawbi H. (2018) Advances in the systemic treatment of melanoma brain metastases. *Ann Oncol* **29**:1509-1520
- Park S.S., Choi Y.W., Kim J.H., Kim H.S., Park T.J. (2021) Senescent tumor cells: an overlooked adversary in the battle against cancer. *Exp Mol Med* **53**:1834-1841
- Pérez-Baños A., Gleisner M.A., Flores I., Pereda C., Navarrete M., Araya J.P., Navarro G., Quezada-Monrás C., Tittarelli A., Salazar-Onfray F. (2023) Whole tumour cell-based vaccines: tuning the instruments to orchestrate an optimal antitumour immune response. *Brit J Cancer* **129**:572-585
- Prieto L.I., Sturmlechner I., Goronzy J.J., Baker D.J. (2023) Senescent cells as thermostats of antitumor immunity. *Sci Transl Med* **15**
- Qin X.Y., Yang T., Xu H.B., Zhang R.Z., Zhao S.Y., Kong L., Yang C.L., Zhang Z.P. (2023) Dying tumor cells-inspired vaccine for boosting humoral and cellular immunity against cancer. *Journal of Controlled Release* **359**:359-372

Ruscetti M., Morris J.P., Mezzadra R., Russell J., Leibold J., Romesser P.B., Simon J., Kulick A., Ho Y.J., Fennell M., *et al.* (2020) Senescence-Induced Vascular Remodeling Creates Therapeutic Vulnerabilities in Pancreas Cancer. *Cell* **181**:424-441.e21

Takasugi M., Yoshida Y., Hara E., Ohtani N. (2023) The role of cellular senescence and SASP in tumour microenvironment. *Febs J* **290**:1348-1361

van Tuyn J., Jaber-Hijazi F., MacKenzie D., Cole J.J., Mann E., Pawlikowski J.S., Rai T.S., Nelson D.M., McBryan T., Ivanov A., *et al.* (2017) Oncogene-Expressing Senescent Melanocytes Up-Regulate MHC Class II, a Candidate Melanoma Suppressor Function. *J Invest Dermatol* **137**:2197-2207

Von Bergwelt-Baildon M.S., Popov A., Saric T., Chemnitz J., Classen S., Stoffel M.S., Fiore F., Roth U., Beyer M., Debey S., *et al.* (2006) CD25 and indoleamine 2,3-dioxygenase are up-regulated by prostaglandin E2 and expressed by tumor-associated dendritic cells in vivo: additional mechanisms of T-cell inhibition. *Blood* **108**:228-237

Wculek S.K., Cueto F.J., Mujal A.M., Melero I., Krummel M.F., Sancho D. (2020) Dendritic cells in cancer immunology and immunotherapy. *Nat Rev Immunol* **20**:7-24

Zhang X.Y., Cui H.Q., Zhang W.J., Li Z.S., Gao J. (2023) Engineered tumor cell-derived vaccines against cancer: The art of combating poison with poison. *Bioact Mater* **22**:491-517

Peer reviews

Reviewer #1 (Public review):

Summary:

The authors aimed to overcome the limitations of whole-tumor-cell vaccines, specifically the weak immunogenicity and rapid clearance often associated with them. They leveraged the unique properties of senescent tumor cells (STCs), which remain metabolically active and secrete chemokines, as a source of antigens. However, to counteract the secretion of the immunosuppressive lipid prostaglandin E2 (PGE2), which is part of the senescence-associated secretory phenotype (SASP), they engineered a hydrogel vaccine formulation (STCs+CLX-Lipo@Gel) containing STCs and liposomal celecoxib (a COX2 inhibitor).

Strengths:

(1) The study is conceptually strong in its approach to leveraging the SASP to improve immunotherapy responses. By selectively inhibiting COX2/PGE2 while preserving the secretion of recruitment chemokines (like CCL2 and CCL5) in the SASP, the authors successfully turn a potentially deleterious cellular state into a therapeutic asset.

(2) Mechanistic Insight: The manuscript provides detailed evidence regarding the mechanism of action. The authors convincingly show that the vaccine restores activity in the NK-DC axis. Specifically, they demonstrate that reducing PGE2 levels enhances NK cell activation (upregulation of NKG2D and NKp46) and promotes the secretion of CCL5 and XCL1 by NK cells, which subsequently recruits cDC1 dendritic cells.

(3) The therapeutic potential is tested across multiple models, including a subcutaneous melanoma model, a difficult-to-treat melanoma brain metastasis model, and an orthotopic pancreatic cancer model. The consistent efficacy across these distinct physiological contexts suggests broad applicability.

Weaknesses:

(1) While the authors successfully inhibit PGE2, the SASP is a complex cocktail of factors. The discussion regarding the long-term presence of these "live" senescent cells is somewhat limited. Although the hydrogel retains cells locally, the potential for other chronic inflammatory factors to eventually promote tumorigenesis or tissue damage in the

surrounding niche warrants careful consideration when translating this approach to patients and may require additional preclinical testing.

(2) The study posits that STCs serve as an antigen reservoir. However, the manuscript would benefit from a clearer distinction between whether the immune system is recognizing senescence-specific neoantigens or simply shared tumor antigens that are being presented more effectively due to the adjuvant effect. The authors briefly touch upon neoantigens in the discussion, but the experimental data primarily measure general anti-tumor responses.

Impact:

This work bridges material science and immunology, offering a practical solution to the immunosuppressive barriers of cell-based vaccines. It provides a platform that could potentially be adapted for various solid tumors.

<https://doi.org/10.7554/eLife.110069.1.sa1>

Reviewer #2 (Public review):

Summary:

Wang et al. examined an engineered whole-tumor-cell vaccine based on senescent tumor cells co-encapsulated with liposomal celecoxib in a chitosan hydrogel. The authors propose that prolonged persistence of senescent cells, combined with COX2/PGE2 inhibition, restores NK-DC crosstalk, enhances cDC1 recruitment, and ultimately drives robust CD8⁺ T-cell-mediated antitumor immunity. The study is nicely executed and clearly presented, with extensive *in vitro* and *in vivo* validation across multiple tumor models, including melanoma brain metastases and orthotopic PDAC. While the overall concept is timely and of potential interest, several mechanistic conclusions are based primarily on correlative evidence and would benefit from additional functional experiments to strengthen causal interpretation and translational relevance.

Strengths:

- (1) Strong conceptual framework
- (2) Impressive breadth of *in vivo* models.
- (3) Clear immunological readouts.
- (4) Innovative combination of senescence biology and biomaterials.

Weaknesses:

- (1) Mechanistic conclusions rely heavily on correlation.
- (2) Lack of functional immune cell depletion studies.
- (3) Limited exploration of long-term safety and antigenic specificity.

Major Critiques:

- (1) The authors emphasize the expansion and activation of cDC1 as a key mechanism linking innate and adaptive immunity, yet it does not directly test whether cDC1 is required for the observed CD8⁺ T-cell responses and tumor control.

The authors should perform experiments using *Batf3*-deficient mice or any other cDC1-depletion strategies to provide important mechanistic validation. If such experiments are not feasible, this limitation should be more clearly acknowledged and discussed.

(2) The authors note that senescence may generate neoantigens distinct from those present in proliferating tumor cells, but the extent to which STC-induced immunity cross-reacts with non-senescent tumor cells is not fully addressed. While it is appreciated that tumor challenge experiments are included, the author should perform a more explicit analysis of antigenic overlap that would strengthen the translational relevance of the approach. For example, they can compare senescence induced by different stimuli or directly assess immune recognition of non-senescent tumor targets, which would help clarify whether the vaccine primarily exploits senescence-specific antigens or broadly shared tumor antigens.

(3) Hydrogel encapsulation clearly extends STC persistence *in vivo*; however, the study provides limited information on the eventual clearance of these cells and the potential implications of prolonged SASP exposure. Given general concerns regarding chronic inflammation associated with senescent cells, additional discussion of long-term local and systemic responses would be helpful. If extended safety analyses are beyond the scope of the current study, the authors should acknowledge the limitation.

(4) The immunological effects are attributed to COX2/PGE2 inhibition, but it remains unclear whether these effects are specific to celecoxib or could reflect formulation-dependent or off-target mechanisms. The authors may perform additional experiments employing an alternative COX2 inhibitor, genetic COX2 suppression, or PGE2 rescue, which could further support the specificity of the COX2/PGE2-dependent mechanism.

<https://doi.org/10.7554/eLife.110069.1.sa0>